

AD-A248 938



PL-TR-91-2139

Environmental Research Papers, No. 1089

②

**Lidar Measurement of Optical Turbulence:
Theory of the Crossed Path Technique**

**Robert R. Beland
J. Krause-Polstorff**

**DTIC
ELECTE
APR 21 1992**
S D D

8 July 1991

Approved for Public Release; Distribution Unlimited

92-10031



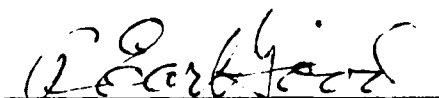
**PHILLIPS LABORATORY
Directorate of Geophysics
AIR FORCE SYSTEMS COMMAND
HANSCOM AIR FORCE BASE, MA 01731-5000**

92 4 20 029

"This technical report has been reviewed and is approved for publication"



DONALD E. BEDO
Chief, Electro-Optical/Measurements Branch



R. EARL GOOD
Director, Optical Environment Division

This report has been reviewed by the ESD Public Affairs Office (PA) and is releasable to the National Technical Information Service (NTIS).

Qualified requestors may obtain additional copies from the Defense Technical Information Center. All others should apply to the National Technical Information Service.

If your address has changed, or if you wish to be removed from the mailing list, or if the addressee is no longer employed by your organization, please notify PL/IMA, Hanscom AFB, MA 01731-5000. This will assist us in maintaining a current mailing list.

Do not return copies of this report unless contractual obligations or notices on a specific document requires that it be returned.

REPORT DOCUMENTATION PAGE			Form Approved OMB No. 0704-0188	
Public reporting burden for this collection of information is estimated to average 1 hour per response, including the time for reviewing instructions, searching existing data sources, gathering and maintaining the data needed, and completing and reviewing the collection of information. Send comments regarding this burden estimate or any other aspect of this collection of information, including suggestions for reducing this burden, to Washington Headquarters Services, Directorate for Information Operations and Reports, 1215 Jefferson Davis Highway, Suite 1204, Arlington, VA 22202-4302, and to the Office of Management and Budget, Paperwork Reduction Project (0704-0188), Washington, DC 20503.				
1. AGENCY USE ONLY (Leave blank)	2. REPORT DATE 8 July 1991	3. REPORT TYPE AND DATES COVERED Scientific, Interim		
4. TITLE AND SUBTITLE Lidar Measurement of Optical Turbulence: Theory of the Crossed Path Technique		5. FUNDING NUMBERS PE 62101F PR 7670 TA 767015 WU 76701520		
6. AUTHOR(S) Robert R. Beland and J. Krause-Polstorff*				
7. PERFORMING ORGANIZATION NAME(S) AND ADDRESS(ES) Phillips Laboratory (GPOA) Geophysics Directorate Hanscom AFB, MA 01731-5000		8. PERFORMING ORGANIZATION REPORT NUMBER PL-TR-91-2139 ERP. No. 1089		
9. SPONSORING / MONITORING AGENCY NAME(S) AND ADDRESS(ES)		10. SPONSORING / MONITORING AGENCY REPORT NUMBER		
11. SUPPLEMENTARY NOTES * Geophysics Scholar				
12a. DISTRIBUTION / AVAILABILITY STATEMENT Approved for public release; distribution unlimited.		12b. DISTRIBUTION CODE		
13. ABSTRACT (Maximum 200 words) The existing measurement capabilities of optical turbulence for IR/optical wavelengths are reviewed. It is shown that no capability exists for simultaneous high spatial and temporal resolution measurements of optical turbulence along an optical path. A general formulation of the remote sensing of optical turbulence is presented, emphasizing the importance of the altitude weighting function, dynamic range requirements and numerical issues. A new approach to lidar remote sensing of turbulence is presented that uses two lidar beams that are viewed by two receivers along a crossed path. The geometric aspects of this theory are discussed and followed by a quantitative formulation based on the Rytov approximation. The approach is similar to the binary star and crossed laser beam methods that have appeared in the literature. The method is based on the intensity covariance of two backscattered spots viewed along crossed paths. The effects of backscatter spot size and receiver averaging are presented. It is shown that the technique is sensitive to the inner scale and is insensitive to the presence of both backscattering spots in both receiver fields of view. The effects of diffraction, turbulence broadening and beam wander are discussed. Criteria are presented for all these effects in the design of a practical system.				
14. SUBJECT TERMS Lidar; Optical turbulence; Remote sensing; Atmospheric turbulence.		15. NUMBER OF PAGES 44		
		16. PRICE CODE		
17. SECURITY CLASSIFICATION OF REPORT UNCLASSIFIED	18. SECURITY CLASSIFICATION OF THIS PAGE UNCLASSIFIED	19. SECURITY CLASSIFICATION OF ABSTRACT UNCLASSIFIED	20. LIMITATION OF ABSTRACT UL	

Contents

1. INTRODUCTION	1
2. METHODS OF MEASUREMENT OF OPTICAL TURBULENCE	2
3. LIDAR APPROACH TO MEASUREMENT OF C_n^2	4
4. THE CROSSED PATH TECHNIQUE	9
4.1 Theory of the Crossed Path Technique	11
4.2 Rytov Theory of the Weighting Function	14
4.3 Finite Receiver and Source Effects	21
4.4 Inner Scale Effects	25
4.5 Overall Weighting Function	29
4.6 Uplink Propagation Effects	32
5. CONCLUSIONS	35
REFERENCES	37

Accession For	
NTIS	CRA&I
DTIC	TAB
Unannounced	
Justification	
By	
Distribution /	
Availability Codes	
Dist	Avail and/or Special
A-1	



Illustrations

1. Geometry of crossed path technique.	10
2. Log amplitude spectrum for the crossed path geometry.	18
3. The crossed path weighting function versus altitude for point backscatterers and point receivers.	20
4. The absolute value of the weighting function is shown in the vicinity of the crossing altitude of 5 km.	20
5. The absolute value of the weighting function is shown in the vicinity of the crossing altitude of 5 km for several values of aperture diameters.	25
6. The maximum value of the weighting function is shown versus the inner scale l_0 .	27
7. The absolute value of the weighting function is shown in the vicinity of the crossing altitude of 5 km for several values of inner scale l_0 .	27
8. The absolute value of the weighting function is shown in the vicinity of the crossing altitude of 500 m showing the magnitude of the total function and the crossed term only.	31
9. The absolute value of the weighting function is shown in the vicinity of the crossing altitude of 500 m showing the magnitude of the total function and the crossed term only.	31

Lidar Measurement of Optical Turbulence: Theory of the Crossed Path Technique

1. INTRODUCTION

With the advent of lasers and their widespread application, the importance of atmospheric optical turbulence has grown. Atmospheric turbulence degrades the propagation of laser beams through the atmosphere. Specifically, wind fluctuations induce density or temperature fluctuations. These temperature fluctuations in turn result in fluctuations of the atmospheric refractive index on scale sizes from a centimeter (or less) to tens of meters. Thus, the refractive index is not homogeneous across a laser beam wavefront larger than approximately a centimeter. The resulting effects of the turbulence are a loss of coherence in the beam, beam broadening, beam wander, intensity fluctuations or scintillations and intensity hot spots within the beam.

Analogous effects occur in passive imaging systems. Mitigation of these effects in lasers and imaging is the goal of adaptive optics compensation methods. Such methods utilize deformable mirrors to compensate for the turbulence induced phase distortions. The performance and characterization of adaptive optics systems requires a knowledge of the fundamental turbulence parameter, C_n^2 , as well as auxiliary meteorological and wind data. These parameters allow specification of the number of mirror actuators, the maximum allowable look-ahead or lag angle, and the bandwidth requirements (or maximum lag time) of the adaptive system. A point that requires emphasis is that these systems require the characterization of an optical path. Such paths are typically of the order of a meter in diameter. Furthermore, such systems require the characterization of the optical path over short time scales. Of course, these paths need to be specified in terms of ensemble averages; the specification of an instantaneous wavefront fluctuation is required only for the entire

propagation path and provides the specific information for performing phase conjugation using adaptive components.

The requirements for the specification of the atmospheric effects are in terms of small volume averages. Such high resolution measurement capability is also needed for more fundamental studies of atmospheric turbulence, specifically, the fine scale spatial and temporal structure of turbulence. These issues of turbulence structure pertain to stationarity, intermittency and the assumption of frozen turbulence. One measurement system that seems (at first consideration) to have the potential for providing such high resolution capability involves the use of lasers for atmospheric remote sensing, that is, lidar. Since the early days of lidar, attempts have been made to use lidar to measure the atmospheric refractive index fluctuations. Very limited success has been achieved.

In this report, the various existing methods for measuring optical turbulence and its parameters are surveyed. This demonstrates the source of our existing knowledge of atmospheric optical turbulence and outlines the limitations of the systems and various measurement issues. A second brief survey of the various approaches to utilizing lidar for C_n^2 profiling follows. The last several sections are devoted to the proposal of a concept for lidar turbulence sensing.

2. METHODS OF MEASUREMENT OF OPTICAL TURBULENCE

Measurements of optical turbulence have been made for several years via radars, in situ instrumentation carried by balloons, and passive optical instrumentation. All the existing methods are limited in various ways.

Radars suffer from high cost, and the large space requirements of the antennas eliminate portability. The maximum vertical resolution is of the order of 150 m in the latest generation Doppler systems¹, but horizontal resolution is dictated by beam divergence and consequently horizontal resolution is altitude dependent. Divergence is usually given in degrees or tens of degrees; the Flatland VHF radar² has a divergence of 3.6 degrees or 626 m at 10 km while the Sousy VHF radar³ has 8 degrees, or 1.4 km horizontal resolution at 10 km. Additionally, radars typically measure a weak signal and require long averaging times; data is usually reported as 15 minute or 1 hour averages. Shorter averaging times are possible by using larger vertical range cells that are as large as 1 km in some cases. Radars measure the average turbulence in a large volume, many times larger than a beam or imaging line of sight. Radars also suffer from two other critical flaws. First, they cannot measure within the first few kilometers above the ground. This region includes the atmospheric boundary layer which has a dominant contribution to various optical effects such as beam wander, broadening and loss of coherence. Second, radars are typically limited to a maxi-

¹Hocking, W.K. (1986) Observation and measurement of turbulence in the middle atmosphere with a VHF radar, *J. Atmos. and Terres. Physics*, **48**:655-670.

²Green, J.L., Beland, R.R., Brown, J.H., Clark, W.L., Eaton, F.D., Favier, L.D., Gage, K.S., Hatch, W.H., Hines, J.R., Murphy, E.A., Nastrom, G.D., Peterson, W.A., VanZandt, T.E., and Warnock, J.M. (1989) Comparisons of Refractivity Measurements from the Flatlands VHF Radar with Other Measurement Techniques, *Proceedings of the 24th Conference on Radar Meteorology*, Tallahassee, FL, March 27-31.

³Eaton, F.D., Peterson, W.A., Hines, J.R., Peterman, K.R., Good, R.E., Beland, R.R. and Brown, J.H. (1988) Comparisons of VHF radar, optical and temperature fluctuation measurements of C_n^2 , ϵ_0 , and θ_0 , *Theor. Appl. Climatol.*, **39**:17-29.

imum range of 20 km, but this is a less serious flaw since turbulence is of less importance in the stratosphere in most applications. This range limitation can be increased by increasing the radar power. Finally, the physical principle in turbulence measurement by radars is the backscattering of the beam by inhomogeneities in the radar refractive index that are the same scale as the wavelength (a VHF radar operates typically at 50 MHz, or $\lambda = 6$ m, which is assumed to be within the inertial range of turbulence). Note that the backscattering results from refractive index fluctuations at radar wavelengths, not optical/IR wavelengths. For radar wavelengths, the refractive index fluctuations are dominated by humidity fluctuations, while for optical/IR wavelengths, the temperature fluctuations are dominant. To convert from radar to optical turbulence requires the measurements of pressure, temperature and humidity. The traditional approach has been to use nearby rawinsonde profiles. These are low resolution (about 1 km vertically) and are not in the same volume. This is a serious drawback if the goal is to use radar to characterize an optical path.

Balloon-borne measurements of optical turbulence have been made for some time⁴. The prevalent technique involves the measurement of temperature fluctuations. Since optical refractive index fluctuations arise entirely from temperature fluctuations, these methods provide a direct measurement of C_n^2 . A further advantage of these measurements is their ability to simultaneously measure meteorological and wind data through the inclusion of a standard radiosonde in the instrument package. The vertical resolution of these methods is determined by statistical estimation considerations and is typically of the order of 50 meters. A major problem with these in-situ methods is that they are not made along any optical path, but rather a path determined by the wind. A second drawback is that, although they provide the highest spatial vertical resolution, balloon-borne measurements also provide the poorest temporal resolution; a balloon flight takes on the order of an hour. Finally, daytime measurements in the stratosphere and upper troposphere present problems⁵ that are likely attributable to solar heating of the temperature probes.

Most passive optical measurement techniques utilize stars as sources and measure some turbulence effect on the propagation of the starlight. Thus, a stellar scintillometer measures the star's intensity fluctuations in a telescope aperture to infer C_n^2 ; an isoplanometer measures isoplanatic angle from a star; and an MTF device measures the transverse coherence length, r_0 , by measuring the blur circle of a star's image in a telescope. These are the most widespread techniques for measuring the vertical structure of turbulence. In principle, they are capable of performing turbulence measurements along an optical path provided there is a conveniently located star. All these techniques are capable of high temporal resolution, limited only by the statistical estimation requirements. However, both the MTF and isoplanometer measure a moment or integral of C_n^2 ; they provide no information about the distribution or layering of turbulence. Thus, their altitude resolution is nonexistent. The scintillometer does provide some altitude-resolved information, but the altitude resolution is poor, of the order of a few kilometers. Further, scintillometers tend to require averaging times of the order of 5 or more minutes. A serious drawback of the scintillometer is its inability to measure turbulence in the first kilometer, a very important region as described earlier. Another limitation of the scintillometer is its restriction to night operation. Both the isoplanometer and the MTF devices have been adapted for daytime use as well.

⁴Brown, J.H., Good, R.E., Bench, P.M. and Faucher, G. (1982) *Sonde Measurements for Comparative Measurements of Optical Turbulence*, Air Force Geophysics Lab., AFGL-TR-82-0079, ADA118740, NTIS.

⁵Walters, D.L., Weitekamp, M.R., Beland, R.R., Good, R.E. and Murphy, E.A. (1990) Single Probe Optical Turbulence Profile Measurement System, Symposium on Propagation Through Turbulence, Annual Meeting of the Opt. Soc. Am., Boston, MA, November 4-9.

This survey of various measurement techniques is intended to present the capabilities and limitations of the various approaches. It emphasizes the methods currently in routine use for atmospheric characterization. The survey is not complete, as there are other methods that have been used. One proposed optical technique uses the scintillation from a satellite-based light source for C_n^2 profiling⁶. Another optical technique that has been presented in the literature utilizes scintillation from binary stars to obtain C_n^2 profiles with up to 1 km vertical resolution⁷. Due to the rarity of binary stars, this technique is limited and cannot be used to measure along a specific optical path. A variation of this technique will be discussed in more detail subsequently in the context of lidar methods. The purpose of this survey has been to demonstrate the capabilities and limitations of existing methods and to show that there is currently no method capable of measuring C_n^2 along a specific optical path with sufficient spatial and temporal resolution.

3. LIDAR APPROACH TO MEASUREMENT OF C_n^2

Given the requirement of characterizing a specific optical path, the use of lidar is an obvious candidate. Lidar methods fall under the category of active optical techniques. The generic lidar approach to any atmospheric measurement is to use a laser pulse that is range gated at the receiver so that the time of arrival of the pulse at the receiver determines the altitude of the backscatterers. A one microsecond pulse gating is typical of lidars and translates into a 150 m vertical resolution. In effect, this receiver gating allows us to treat the lidar as an array of sources separated by 150 m along the optical path.

A general formulation of a lidar approach to C_n^2 measurement will be presented. A lidar system will measure some optical effect, say g , from the gated return at altitude z_i . In general, the effect g will be determined by the entire optical path from the transmitter ($z = 0$) to the backscatterer ($z = z_i$) and then back to the receiver ($z = 0$). The optical effect can be written as an integral along the optical path:

$$g(z_i) = \int_0^{z_i} C_n^2(h) W(\lambda, z_i, h) dh, \quad (1)$$

where $W(\lambda, z_i, h)$ is the particular optical effect's path weighting function at wavelength λ , observed at $z = 0$ and backscattered at z_i . The weighting function measures the contribution to this effect arising from optical turbulence at $z = h$. We can write this down as a sum of integrals over the range gates as:

$$\begin{aligned} g(z_i) &= \sum_{j=1}^i \int_{z_{j-1}}^{z_j} C_n^2(h) W(\lambda, z_i, h) dh \\ &= \sum_{j=1}^i C_n^2(z_j) \int_{z_{j-1}}^{z_j} W(\lambda, z_i, h) dh, \end{aligned} \quad (2)$$

⁶Krause-Polstorff, J. and Walters, D.L. (1990) Refractive turbulence profiling using an orbiting light source, *Appl. Opt.*, **29**:1877-1885.

⁷Azouit, M., Vermin, J., Barletti, R., Ceppatelli, G., Righini, A. and Speroni, N. (1980) Remote sensing of atmospheric turbulence by means of a fast optical method: A comparison with simultaneous *in situ* measurements, *J. Appl. Meteor.*, **19**:834-838.

where $C_n^2(z_j)$ is the weighted-average C_n^2 over the altitude bin (z_{j-1}, z_j) defined by

$$C_n^2(z_j) = \frac{\int_{z_{j-1}}^{z_j} C_n^2(h) W(\lambda, z_j, h) dh}{\int_{z_{j-1}}^{z_j} W(\lambda, z_j, h) dh} \quad (3)$$

Strictly, we should write $C_n^2(z_j, z_i)$ to show the dependence on z_i . However, the dependence of the weighted average on z_i is assumed to be weak over the range (z_{j-1}, z_j) . Additionally, if C_n^2 is constant over (z_{j-1}, z_j) , the dependence disappears and it will be assumed that C_n^2 is constant over (z_{j-1}, z_j) . This last form allows us to write the result in the suggestive matrix form:

$$g(z_i) = \sum_{j=1}^i W_{ij} C_n^2(z_j), \quad (4)$$

or in terms of vectors \underline{G} and \underline{C} and matrix W :

$$\underline{G} = W \underline{C}, \quad (5)$$

where the matrix W has elements W_{ij} defined by

$$W_{ij} = \int_{z_{j-1}}^{z_j} W(\lambda, z_i, h) dh, \quad (6)$$

and the vector elements of \underline{G} and of \underline{C} are $g(z_i)$ and $C_n^2(z_j)$, respectively. The solution giving $C_n^2(z_j)$ in terms of the measured quantities $g(z_i)$ is then formally given by:

$$\underline{C} = W^{-1} \underline{G}. \quad (7)$$

The formulation is readily extended to included measurement errors in terms of an error vector \underline{e} . This yields a formal least squares type problem whose solution properties are the critical question. The numerical stability and problem of ill-conditioning are of central importance. In general, the matrix W has elements that satisfy

$$W_{ij} = 0 \text{ for } j > i. \quad (8)$$

This simply states that turbulence at altitudes higher than the backscatter volume has no effect. All the upper half matrix elements are zero and the formulation gives a triangular system of equations. The formal solution of this system of equations is given by⁸

$$C_n^2(z_i) = (W_{ii})^{-1} \left[g(z_i) - \sum_{j=1}^{i-1} W_{ij} C_n^2(z_j) \right]. \quad (9)$$

There exist two broad approaches to turbulence measurements via lidar. The two cases are where the optical effect arises from phase distortions and where the effects arises from amplitude

⁸Dahlquist, G. and Bjorck, A. (1974) *Numerical Methods*, Prentice-Hall, Englewood Cliffs, N.J.

distortions; these are considered in turn. To simplify the discussion, it is assumed that the backscattering volume has a cross-sectional area (transverse to the propagation direction) that is sufficiently small so that it can be considered a point source. The complexity of finite backscatter spot size, although important in describing the optical effect, is not important in this treatment, as we are presenting "first order" considerations. The second major simplifying assumption is that there are no turbulence effects on the uplink; that is, turbulence only effects the downlink propagation from the backscatterers to the receiver. This is clearly unrealistic, but again, we wish to discuss issues associated with a "first order" approach. The effect of these two assumptions is that we are addressing the following problem: we have a linear array of point sources separated vertically by a distance Δ , and we seek to determine C_n^2 vertically from this array.

Consider first a phase process, chosen to be image dancing for concreteness. For a point source at z observed by a receiver located at 0 and of diameter D , the mean square wander, $\langle \delta^2 \rangle$, is given by

$$\langle \delta^2(z) \rangle = 2.91 f^2 D^{-1/3} \int_0^z C_n^2(\eta) [1-(\eta/z)]^{5/3} d\eta. \quad (10)$$

The expression gives the wander measured in the focal plane of the receiver of focal length f , provided the receiver diameter is within the inertial range. In our formulation, we have that

$$g(z_i) = \langle \delta^2(z_i) \rangle, \quad (11)$$

$$\begin{aligned} W_{ij} &= \int_{z_{j-1}}^{z_j} W(\lambda, z_i, h) d\eta \\ &= 2.91 f^2 D^{-1/3} \int_{z_{j-1}}^{z_j} [1-(\eta/z)]^{5/3} d\eta. \end{aligned} \quad (12)$$

This can be evaluated explicitly to give

$$W_{ij} = 2.91 f^2 D^{-1/3} (3z_j/8) \left\{ \left[1-(z_{j-1}/z_i) \right]^{8/3} - \left[1-(z_j/z_i) \right]^{8/3} \right\}. \quad (13)$$

A case of special interest is where $j \ll i$, that is, the altitude range bin is far from the backscatter region. An expansion yields

$$W_{ij} \approx 2.91 f^2 D^{-1/3} (z_j - z_{j-1}) = 2.91 f^2 D^{-1/3} \Delta, \quad (14)$$

where $\Delta = (z_j - z_{j-1})$ is the width of the range gate. Note that the matrix elements far from the diagonals do not depend on i or j .

The other case of special interest is the first bin in front of the source. This gives one of the diagonal elements of the matrix W , that is, the element W_{ii} :

$$W_{ii} = 1.09 f^2 D^{-1/3} z_i^{-5/3} \Delta^{8/3} = 1.09 f^2 D^{-1/3} \Delta i^{-5/3}, \quad (15)$$

where $z_i = i\Delta$. The formal mathematical problem with this method is apparent from the following. Consider the ratio of the diagonal element W_{ii} to an off diagonal element W_{ij} where $j \ll i$. As an example, let $\Delta = 150$ m and let $z_i = 10$ km. Then

$$W_{ii}/W_{ij} = 0.375 (\Delta/z_i)^{5/3} \approx 9 \times 10^{-4}. \quad (16)$$

The peculiar property of the matrix is that a diagonal element is smaller than any other element in its row. The diagonal elements can be smaller by several orders of magnitude. This results from the physical path weighting, whereby the path is weighted the least in front of the source, zero at the source and increases with distance away from the source.

The numerical problems in this method readily exhibit themselves. Atmospheric turbulence (and hence phase distortions) varies by four orders of magnitude from a C_n^2 value of about 10^{-13} near the ground to 10^{-17} in the troposphere. Optical turbulence can vary by as much as 3 orders of magnitude in the troposphere, depending on whether there is a strong turbulent layer present. The combination of the range of turbulence with the wide range in the matrix W requires a dynamic range of more than 10^7 in the receiver detector to avoid the numerical problems. Alternatively, the dynamic range requirements can be reduced by limiting the resolution.

Although this calculation has been performed for a specific phase effect, similar results will likely arise for other phase effects as well. The problems arise from both the path weighting problem and the sensitivity of phase effects to large eddies. These two effects are closely related. An alternative approach that avoids the dominance of large eddies involves those effects based on scintillation. For a point source at altitude z_i , the variance of log-amplitude observed by a receiver on the ground is given by:

$$\sigma_\chi^2(z_i) = 0.56 k^{7/6} \int_0^{z_i} C_n^2(\eta) (\eta/z_i)^{5/6} (z_i - \eta)^{5/6} d\eta. \quad (17)$$

Note that the weighting is zero both at the receiver and at the source and is symmetric about the path midpoint. Exactly as in the phase approach, we can construct a set of triangular equations corresponding to a range-resolved lidar measurement. The resulting matrix W gives rise to the same numerical issues as the phase example.

A further complication arises for both these first-order approaches if the uplink effects are included, that is, the propagation from the laser to the backscattering region. In the case of the phase measurement of angle of arrival, the uplink propagation produces beam wander at the backscattering altitude z_i . For a collimated transmitter of diameter a , the mean square wander at z_i is given for propagation from $z=0$ to z_i by⁹

$$\langle \rho_c^2 \rangle \approx 6.08 z_i^2 a^{-1/3} \int_0^{z_i} C_n^2(h) dh. \quad (18)$$

The illumination of the backscattering region is changing as a result of the beam centroid wander. The image of the backscattered spot wanders in the image plane as a result of the uplink beam wander and the downlink image dancing. Clearly, the uplink propagation modifies the path weighting function. The modification is not a straightforward sum of the uplink and downlink; the up and down paths are nearly identical, and strongly statistically dependent. Since turbulence can be regarded as frozen over the propagation time, the entire propagation occurs within an isoplanatic patch. The downlink performs, to some degree, a phase conjugation of the uplink phase distortions, thereby reducing the dancing. If instead of backscattering, a retroreflector is used at

⁹Sasiela, R.J. (1988) *A Unified Approach to Electromagnetic Wave Propagation in Turbulence and the Evaluation of Multiparameter Integrals*. Technical Report No. 807, MIT/Lincoln Laboratory.

altitude z_i , the down beam would be a phase conjugated version of the up beam and nearly perfect conjugation (except for diffraction) would be observed at the detector with almost no wander. For backscattering, the down beam is a spherical wave (or incoherent superposition of spherical waves) while the up beam is a collimated, partially coherent beam wave. The conjugation is less than perfect. This is a difficult problem whose solution has not been achieved. It is clear that the path weighting function has been modified to a considerable extent by the inclusion of the uplink propagation.

If this overall path weighting function were known, it is still likely that certain difficulties in a phase approach would remain. The problem of greatest concern is the requirement of very large dynamic range. As the above equations show, angle of arrival fluctuations are directly proportional to C_n^2 ; since C_n^2 varies by more than 10^3 , so do phase effects. In addition, phase effects are dominated by large turbulence, which occurs near the aperture and in the boundary layer. Measurements from backscattering above the boundary layer will include these large distortions, and the contribution from above the boundary layer will be swamped by the larger contribution from below.

Closely related to these problems are the noise sources inherent in a phase measurement approach. One source is laser instabilities that contribute a jitter to the propagation. A second source is mechanical vibration in the transmitter or receiver that also contributes a jitter and results in some image dancing. In the presence of noise, the numerical considerations of stability become of great importance.

The value of scintillation-based approaches is that some of the problems inherent in the phase approach are not significant. The uplink wander of the beam does not matter, provided the spot remains in the detector field of view. The same considerations apply to other sources of jitter, such as laser instabilities and vibrations. The central concept in log-amplitude based approaches is that they are insensitive to the large scale sizes and the important scale is the Fresnel scale, given by $(\lambda z)^{1/2}$, which is typically of the order of centimeters. Scintillation along an optical path is not dominated by the largest turbulence, but by a combination of the value of C_n^2 and the turbulent layer's Fresnel scale.

A key issue in scintillation is that the conjugation considerations of the up and down links are a negligible consideration. This is not to imply that scintillation approaches are not affected by the uplink propagation. The uplink propagation results in intensity fluctuations of the light incident on the backscatterers. There are two aspects to this effect. The first is the fluctuation of the total incident energy on the backscatterers. Scintillation approaches tend to calculate the mean square average of the log intensity or log amplitude and for weak scintillation, these can be shown to be virtually the same as the normalized intensity variance. The approach performs a normalization for the overall intensity fluctuation. The second aspect pertains to scintillation within the finite spot size of the beam at the scatterers; the uplink scintillation will result in intensity hot spots at the scatterers. The problem is that of scintillation from an extended source. This problem is a second order effect and is discussed in the following. Closely related is the important problem of the beam broadening due to the uplink distortions. This reduces the overall scintillation and changes the path weighting. Indeed, the use of different size sources and receivers is a fundamental design principle in the horizontal scintillometer and its variants¹⁰. Certain effects resulting from beam broadening can be described. The path weighting function for scintillation is a broad peak,

¹⁰Ochs, G.R. and Wang, T. (1978) Finite aperture scintillometer for profiling wind and C_n^2 , *Appl. Opt.*, 17:3774-3778.

with zeroes at the transmitter and receiver. The location of the center of the peak may be changed by adjustment of the receiver and transmitter diameters, but the peaks will remain fairly broad and the overall scintillation will be reduced from the point source and receiver case. Furthermore, a practical lidar system places severe constraints and limitations on the amount of adjustment possible in the receiver and transmitter diameters. These considerations will result in the previously stated numerical issues: a very large dynamic range in the receiver is required. Very limited altitude resolution would be achievable.

4. THE CROSSED PATH TECHNIQUE

The ideal lidar measurement method would be based on an optical property that has a very sharply peaked path weighting function and would be minimally effected by laser instabilities, system vibrations and uplink beam wander. It would also measure an optical effect that yields a reasonably strong signal. The first requirement insures numerical robustness. It has also been suggested in the previous section that a phase-based approach would not meet any of these requirements and even if the phase conjugation theory for the uplink/downlink problem were completed, the sensitivity to system jitter would remain. It appears that a scintillation-based approach holds a higher degree of promise of success.

An approach is presented that uses a scintillation method and produces a sharp path weighting function. This approach is an adaptation to lidar of the binary-star methods for passive remote sensing^{7,11}. The method was also suggested¹² as a means of remote sensing across a horizontal distance and a variant has been used to measure turbulence in fluid flow¹³. The strength of the method is that the path weighting is determined by geometric factors. In Figure 1, two parallel beams, separated by a distance S_0 , are backscattered at an altitude z . The backscattered spots are viewed by two receivers of diameter D , separated by S , in such a way that their viewing paths cross. If the altitude of the backscatterers is given by z , geometric considerations show that the two observation paths cross at an altitude h given by

$$h = Sz/(S+S_0) = z/(1+S_0/S). \quad (19)$$

This simple equation demonstrates the relation between the backscattering altitude, the crossing altitude and the receiver and scatterer separations. The second form shows that it is the ratio of the backscatter and receiver separation that determine the crossing altitude. In a lidar implementation based on this approach, there is considerable flexibility in adjusting these parameters.

Each receiver measures the fluctuating intensity from one of the sources and this scintillation is determined by the optical turbulence along the entire path. However, if the correlation of the intensities at the two receivers is measured, it is determined solely by the turbulence in com-

¹¹Vernin, J. and Pelon, J. (1986) Scidar/lidar description of a gravity wave and associated turbulence: preliminary results, *Appl. Opt.*, **25**:2874-2877.

¹²Wang, T., Clifford, S.F. and Ochs, G.R. (1974) Wind and Refractive-Turbulence Sensing Using Crossed Laser Beams, *Appl. Opt.*, **13**:2602-2608.

¹³Fisher, M.J., and Krause, F.J. (1967) The crossed-beam correlation technique, *J. Fluid Mech.*, **28**:705-717.

mon, that is, the turbulence in the volume of overlap of the viewing geometries. It is clear that the path weighting function for this correlation is sharply peaked at the center of the volume of overlap, given by h , and is essentially zero outside of this. The geometry can be used to provide insight into the parametric dependencies of the width of the weighting function and hence the altitude resolution of the technique. If Δ_1 and Δ_2 are respectively the lower and upper limits of overlap as shown in Figure 1, then

$$\begin{aligned}\Delta_1 &= D(z-h)/(S+S_0-D), \\ \Delta_2 &= D(z-h)/(S+S_0+D).\end{aligned}\tag{20}$$

Since in practice, the receiver diameter would be smaller than the other horizontal dimensions, the approximation $D \ll S, S_0$ shows

$$\Delta \approx \Delta_1 \approx \Delta_2 \approx D(z-h)/(S+S_0).\tag{21}$$

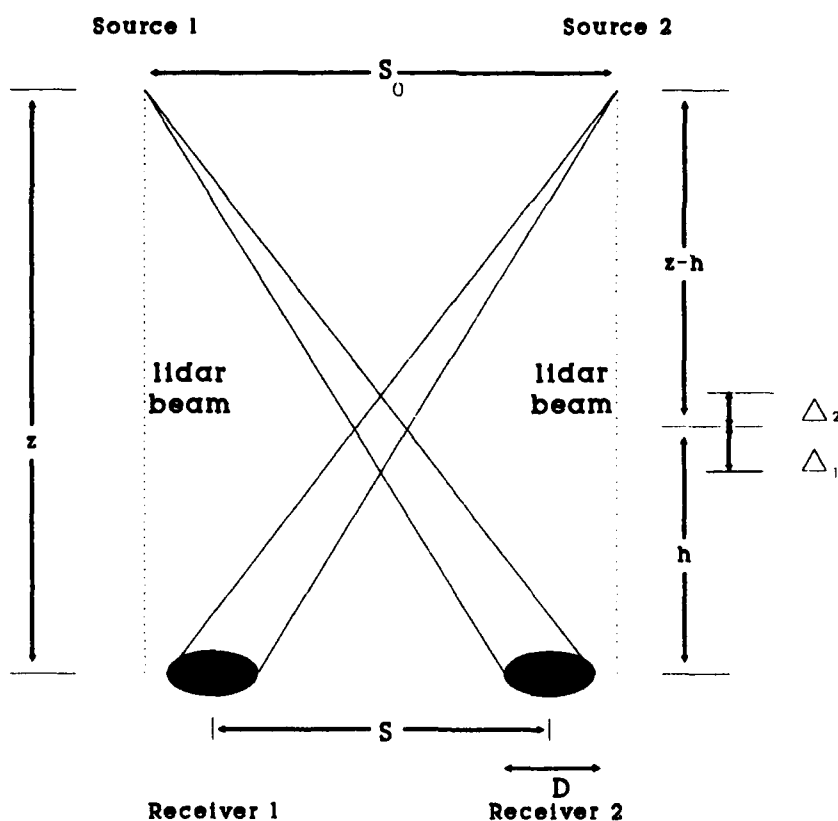


Figure 1. Geometry of crossed path technique. The viewing paths of the two receivers are crossed as shown. The two outgoing lidar beams are not crossed and are shown by the dotted lines.

This is equivalent to assuming that the spherical spreading of the light is negligible over the volume of overlap, and thus the light cones from the sources can be treated as cylinders in the crossing region. As a numerical example, consider backscattering from a 10 km altitude. If the source and receiver separation are 1 m, the crossing altitude is 5 km and a 10 cm receiver gives a geometric overlap of ± 250 m. The vertical resolution is 500 m.

It should be emphasized that these geometric relations are primarily heuristic and are given to demonstrate the parametric dependencies and semi-quantitative behavior of the solution. A more thorough and formal solution based on the Rytov theory is presented shortly. The geometric theory provides only semi-quantitative information about the path weighting function and its width, while the Rytov theory specifies the function completely. For the numerical example just given, it will be shown that the Rytov theory yields much sharper path weighting, and hence higher resolution, than the geometric theory.

4.1 Theory of the Crossed Path Technique

This section demonstrates the key relationship between the intensity covariance, which is the measurable quantity, and the covariance of log amplitude, which is related to the crossing volume. Let I_1 and I_2 be the intensity received by the two detectors shown in Figure 1. In the more general case, both sources are in the field of view of the two receivers. This minor complication is accounted for later. In the present derivation, we assume that each receiver sees only one source and that the observation paths cross as suggested in Figure 1. The covariance between the two receivers separated by S is

$$\begin{aligned} C_I(S) &= \langle (I_1 - \langle I_1 \rangle)(I_2 - \langle I_2 \rangle) \rangle \\ &= \langle I_1 I_2 \rangle - \langle I_1 \rangle \langle I_2 \rangle, \end{aligned} \quad (22)$$

where the brackets indicate ensemble averaging. By definition of log amplitude, χ , we have that

$$I_1(x, y) = I_{01}(x, y) e^{2\chi_1(x, y)}, \quad (23)$$

where $I_{01}(x, y)$ is the intensity at (x, y) in the absence of turbulence. The analogous relation exists for $I_2(x', y')$. Upon substitution into the covariance, we get

$$C_I(S) = I_{01}(x, y) I_{02}(x', y') \{ \langle e^{2[\chi_1(x, y) + \chi_2(x', y')]} \rangle - \langle e^{2\chi_1(x, y)} \rangle \langle e^{2\chi_2(x', y')} \rangle \}, \quad (24)$$

where S is the distance between (x, y) and (x', y') . There is considerable theoretical and experimental evidence that in the weak scintillation case χ is a normal (Gaussian) random variable from which it follows that

$$\langle I \rangle = I_0 \langle e^{2\chi} \rangle = I_0 e^{2\langle \chi \rangle + 2\sigma_\chi^2}, \quad (25)$$

where σ_χ^2 is the variance of log amplitude. Since both χ_1 and χ_2 are normal, so is their sum, χ_+ , and we have that

$$\langle e^{2\chi_+} \rangle = e^{2\langle \chi_+ \rangle + 2\sigma_{\chi_+}^2}, \quad (26)$$

where

$$\langle \chi_+ \rangle = \langle \chi_1 \rangle + \langle \chi_2 \rangle, \quad (27)$$

and

$$\sigma_{\chi_+}^2 = \sigma_{\chi_1}^2 + \sigma_{\chi_2}^2 + 2C_\chi(S). \quad (28)$$

This last form introduces the covariance at a separation S of the log amplitude at receivers 1 and 2, $C_\chi(S)$, which is formally defined by

$$\begin{aligned} C_\chi(S) &= \langle (\chi_1 - \langle \chi_1 \rangle)(\chi_2 - \langle \chi_2 \rangle) \rangle \\ &= \langle \chi_1 \chi_2 \rangle - \langle \chi_1 \rangle \langle \chi_2 \rangle. \end{aligned} \quad (29)$$

Putting these results together yields

$$\langle e^{2\chi_+} \rangle = e^{2\langle \chi_1 \rangle + 2\langle \chi_2 \rangle + 2\sigma_{\chi_1}^2 + 2\sigma_{\chi_2}^2 + 4C_\chi(S)}. \quad (30)$$

Substituting these results produces

$$\begin{aligned} C_I(S) &= I_{01} I_{02} \left\{ e^{2\langle \chi_1 \rangle + 2\langle \chi_2 \rangle + 2\sigma_{\chi_1}^2 + 2\sigma_{\chi_2}^2 + 4C_\chi(S)} - e^{2\langle \chi_1 \rangle + 2\langle \chi_2 \rangle + 2\sigma_{\chi_1}^2 + 2\sigma_{\chi_2}^2} \right\} \\ &= I_{01} I_{02} e^{2\langle \chi_1 \rangle + 2\langle \chi_2 \rangle + 2\sigma_{\chi_1}^2 + 2\sigma_{\chi_2}^2} \left\{ e^{4C_\chi(S)} - 1 \right\} \\ &= \langle I_1 \rangle \langle I_2 \rangle \left\{ e^{4C_\chi(S)} - 1 \right\}. \end{aligned} \quad (31)$$

Approximating the exponential for weak scintillations gives

$$C_I(S) \approx 4\langle I_1 \rangle \langle I_2 \rangle C_\chi(S). \quad (32)$$

This is a key equation in our formulation which demonstrates that the intensity covariance between the two receiver outputs is reduced to the problem of evaluating the log amplitude covariance. It is worth emphasizing that this derivation requires only the assumption of normality of the log amplitude. Fried¹⁴ performs the same derivation but also includes the requirement of conservation of energy. Since optical turbulence does not dissipate the optical energy, conservation of energy is implemented by requiring that $\langle I \rangle = I_0$, which in turn implies that for log normal variables, $\langle \chi \rangle = -\sigma_\chi^2$. As the above derivation shows, the relation between the covariances of intensity and log amplitude does not require that conservation of energy be utilized. It is clear that this restriction on $\langle \chi \rangle$ conflicts with the Rytov approximation which produces $\langle \chi \rangle = 0$ and the normality of χ . The Rytov theory is only an approximation resulting from a perturbation expan-

¹⁴Fried, D.L. (1967) Aperture Averaging of Scintillations, *J. Opt. Soc. Am.*, **57**:169-175.

sion while the requirement of conservation of energy is exact. Mixing different orders of approximation in theory is to be avoided since it may lead to contradictions. Since the theory of the crossed path technique is to be developed from the Rytov theory and the conservation of energy requirement is unnecessary, only those assumptions that are part of the Rytov approximation are assumed.

Before turning to the derivation of the log amplitude covariance, it is shown that the theory is readily expanded to accommodate the complication of both sources in the field of view of both receivers. Let I_1 and I_2 denote the total intensity in receiver 1 and 2 respectively. In the case of independent sources, the total intensity results from an incoherent superposition of the individual fields:

$$\begin{aligned} I_1 &= I_{11} + I_{12}, \\ I_2 &= I_{21} + I_{22}, \end{aligned} \tag{33}$$

where I_{ij} is the intensity from the j^{th} source at the i^{th} receiver. Substituting and performing algebra yields the following form for the covariance of the intensity between receivers 1 and 2:

$$\begin{aligned} C_I(S) &= \langle I_1 I_2 \rangle - \langle I_1 \rangle \langle I_2 \rangle \\ &= [\langle I_{11} I_{21} \rangle - \langle I_{11} \rangle \langle I_{21} \rangle] + [\langle I_{12} I_{22} \rangle - \langle I_{12} \rangle \langle I_{22} \rangle] \\ &\quad + [\langle I_{12} I_{21} \rangle - \langle I_{12} \rangle \langle I_{21} \rangle] + [\langle I_{11} I_{22} \rangle - \langle I_{11} \rangle \langle I_{22} \rangle]. \end{aligned} \tag{34}$$

In this expression, the terms have been grouped suggestively. The first term is the covariance of source 1 at receivers 1 and 2. This is the same as the covariance of source one for two points in the observation plane separated by S (if the receivers are regarded as point receivers). Now, the intensity covariance of a turbulent layer goes to zero for separations larger than the Fresnel scale¹⁵. The receiver separation, S , will in practice be of the order of a meter, while the Fresnel scale of any turbulent layer will be of the order of centimeters. Therefore, it is to be expected that in the lidar formulation, the first term is small. Similarly, the second term is the covariance of source 2 at a separation S , and is also small. The third term is the crossed path term; it is the covariance of source 1 at receiver 2 with source 2 at receiver 1. It is given by the earlier result:

$$\langle I_{12} I_{21} \rangle - \langle I_{12} \rangle \langle I_{21} \rangle \approx 4 I_{01} I_{02} C_\chi(S). \tag{35}$$

The last term is the covariance of source 1 at receiver 1 with source 2 at receiver 2. This is the uncrossed path, and represents the covariance of independent sources. Again, provided the paths are separated by more than a Fresnel scale, this term is also very small. Thus, in the lidar implementation, the additional terms resulting from both sources in the field of view of both receivers are expected to be small. The smallness of these terms in the above arguments is relative to their respective maximums, and not relative to the magnitude of the crossed path term. Although the above

¹⁵Clifford, S.F. (1978) The Classical Theory of Wave Propagation in a Turbulent Medium, Chapter 2, in *Laser Beam Propagation in the Atmosphere*, J.W. Strohbehn, Ed., Springer-Verlag, New York.

arguments indicate that in a lidar implementation it does not matter whether both sources are in the field of view of the receivers, this claim will be addressed in a more quantitative fashion in a subsequent section. This robustness is a very desirable property. Because of this property, all the following derivations will assume that only one source is seen by each receiver. In contrast, the binary star technique uses receiver separation of the same order or smaller than the Fresnel scale, so the additional covariance terms must be included.

4.2 Rytov Theory for the Weighting Function

The theory of the crossed path technique has been reduced to that of the covariance of the log amplitude for the propagation. The Rytov solution to the wave equation is written in the general form¹⁶

$$\psi(r) = k^2 [2\pi E_0(r)]^{-1} \int \frac{e^{ik|r-r'|}}{|r-r'|} n_1(r') E_0(r') dr', \quad (36)$$

where $\psi = \chi + i\phi$, χ is the log amplitude and ϕ is the phase and thus, $\chi = \text{Re}(\psi)$. In this equation, k is the optical wavenumber ($2\pi/\lambda$), r is the vector observation point, $E_0(r')$ is the source amplitude at r' , and $n_1(r')$ is the refractive index fluctuation at r' . By definition of the refractive index fluctuations, $\langle n_1(r') \rangle = 0$, from which it follows from the Rytov approximation that $\langle \psi \rangle = \langle \chi \rangle = \langle \phi \rangle = 0$. Thus, the covariance of the log amplitude reduces to

$$C_\chi(S) = \langle \chi_1 \chi_2 \rangle. \quad (37)$$

If the distance to the observation point is greater than any lateral dimension in the problem, the Fresnel approximation can be applied and so the Rytov solution can be written in general as

$$\psi(r) = k^2 [2\pi E_0(r)]^{-1} \int \frac{e^{ik(\mathbf{p} - \mathbf{p}')^2/[2(z-z')]} }{(z-z')} n_1(r') e^{ik(z-z')} E_0(r') dr', \quad (38)$$

where \mathbf{p} is a vector in the plane transverse to the direction of propagation, which is taken to be the z -axis. The source is specified by $E_0(r)$, the source amplitude observed at vector r . For a point source, located at vector r_0 ,

$$E_0(r) = E_0 \frac{e^{ik|r-r_0|}}{4\pi|r-r_0|}. \quad (39)$$

If the point source is located at $z = 0$ and transverse vector \mathbf{p}_0 , the Fresnel approximation can also be applied to the source to give

$$E_0(r) \approx E_0 \frac{e^{ikz}}{4\pi z} e^{ik|\mathbf{p}-\mathbf{p}_0|^2/2z}. \quad (40)$$

¹⁶Tatarski, V.I. (1961) *Wave Propagation in a Turbulent Medium*, McGraw-Hill, New York.

Substitution into the Rytov solution gives

$$\psi(r) = (k^2/2\pi) z e^{-ik|\mathbf{p}-\mathbf{p}_0|^2/2z} \int \frac{e^{ik|\mathbf{p}-\mathbf{p}'|^2/2(z-z')}}{z(z-z')} e^{ik|\mathbf{p}'-\mathbf{p}_0|^2/2z'} n_1(r') dz' d\mathbf{p}'. \quad (41)$$

After some tedious algebraic manipulation, it can be shown that

$$|\mathbf{p}-\mathbf{p}_0|^2/z + |\mathbf{p}-\mathbf{p}'|^2/(z-z') + |\mathbf{p}'-\mathbf{p}_0|^2/z' = |\mathbf{p}'-\gamma\mathbf{p}+(1-\gamma)\mathbf{p}_0|^2/\gamma(z-z'), \quad (42)$$

where we have introduced $\gamma = z'/z$. Making this substitution gives

$$\psi(r) = (k^2/2\pi) \int \frac{e^{ik|\mathbf{p}'-\gamma\mathbf{p}-(1-\gamma)\mathbf{p}_0|^2/2\gamma(z-z')}}{\gamma(z-z')} n_1(r') dz' d\mathbf{p}'. \quad (43)$$

To simplify this further, the spectral expansion for the refractive index fluctuations is introduced:

$$n(\mathbf{p}, z) = \int d\mathbf{v}(\mathbf{K}, z) e^{i\mathbf{K}\cdot\mathbf{p}}, \quad (44)$$

where \mathbf{K} is the two-dimensional vector spatial wavenumber. If this substitution is made, the following integral over \mathbf{p}' results:

$$I_1 = \int e^{i\mathbf{K}\cdot\mathbf{p}} e^{ik|\mathbf{p}'-\gamma\mathbf{p}-(1-\gamma)\mathbf{p}_0|^2/2\gamma(z-z')} d\mathbf{p}'. \quad (45)$$

By a change of variable to \mathbf{p}_* where $\mathbf{p}_* = \mathbf{p}'-\gamma\mathbf{p}-(1-\gamma)\mathbf{p}_0$, this becomes

$$I_1 = e^{i\mathbf{K}\cdot[\gamma\mathbf{p}+(1-\gamma)\mathbf{p}_0]} \int e^{i\mathbf{K}\cdot\mathbf{p}_*} e^{ik|\mathbf{p}_*|^2/2\gamma(z-z')} d\mathbf{p}_*. \quad (46)$$

$$= 2\pi e^{i\mathbf{K}\cdot[\gamma\mathbf{p}+(1-\gamma)\mathbf{p}_0]} \int J_0(K\rho_*) e^{ik\rho_*^2/2\gamma(z-z')} \rho_* d\rho_*. \quad (47)$$

$$= 2\pi e^{i\mathbf{K}\cdot[\gamma\mathbf{p}+(1-\gamma)\mathbf{p}_0]} \left\{ [i\gamma(z-z')/k] e^{-i\gamma(z-z')K^2/2k} \right\}. \quad (48)$$

The first step in this integration converts the integral over vector \mathbf{p} into an integral over scalar ρ and angle. This allows the introduction of the zeroth order Bessel function via its integral representation¹⁷. The next step is performed by recognizing that the integral is in the form of a Fourier-Bessel (or Hankel) transform of a Gaussian¹⁸. Using this result, we have the general Rytov solution for a point source at arbitrary vector position, \mathbf{p}_0 , in the plane $z = 0$ and observed at position vector $\mathbf{r} = (\mathbf{p}, z)$:

$$\psi(r) = ik \int dz' \int d\mathbf{v}(\mathbf{K}, z') e^{i\mathbf{K}\cdot[\gamma\mathbf{p}+(1-\gamma)\mathbf{p}_0]} e^{-i\gamma(z-z')K^2/2k}, \quad (49)$$

¹⁷ Mathews, J. and Walker, R.L. (1970) *Methods of Mathematical Physics*, 2nd edn., W.A. Benjamin, Reading, MA.

¹⁸ Bracewell, R.N. (1978) *The Fourier Transform and Its Applications*, 2nd edn., McGraw-Hill, N.Y.

where the real part provides the log amplitude. Note that a point source at the origin, $\mathbf{p}_0 = 0$, gives the expression usually stated as the Rytov spherical wave solution. It follows from this that the log amplitude is given by

$$\chi(r) = (1/2)[\psi + \psi^*] \quad (50)$$

$$= k \int dz' \int dv(\mathbf{K}, z') e^{i\mathbf{K} \cdot [\gamma \mathbf{p} + (1-\gamma) \mathbf{p}_0]} \sin[\gamma(z-z')K^2/2k]. \quad (51)$$

The requirement that the refractive index fluctuations be real is used to obtain the last expression. Specifically, the realness of n in the spectral expansion implies that

$$dv(\mathbf{K}, z) = dv^*(-\mathbf{K}, z). \quad (52)$$

The Rytov solution for each receiver can be written as

$$\chi_1 = \chi(r_1) = k \int dz' \int dv(\mathbf{K}, z') e^{i\mathbf{K} \cdot [\gamma \mathbf{p}_1 + (1-\gamma) \mathbf{p}_{02}]} \sin[\gamma(z-z')K^2/2k], \quad (53)$$

$$\chi_2 = \chi(r_2) = k \int dz'' \int dv(\mathbf{K}', z'') e^{i\mathbf{K}' \cdot [\gamma' \mathbf{p}_2 + (1-\gamma') \mathbf{p}_{01}]} \sin[\gamma'(z-z'')K'^2/2k]. \quad (54)$$

where $\gamma' = z''/z$. The subscripts are chosen to emphasize the crossed path: source 2 is measured at receiver 1 and source 1 at receiver 2. Taking the product of these two expressions and performing ensemble averages gives

$$\begin{aligned} \langle \chi_1 \chi_2 \rangle &= k^2 \int dz' dz'' \int \langle dv(\mathbf{K}, z') dv(\mathbf{K}', z'') \rangle \\ &\quad e^{i\mathbf{K} \cdot [\gamma \mathbf{p}_1 + (1-\gamma) \mathbf{p}_{02}]} \sin[\gamma(z-z')K^2/2k] e^{i\mathbf{K}' \cdot [\gamma' \mathbf{p}_2 + (1-\gamma') \mathbf{p}_{01}]} \sin[\gamma'(z-z'')K'^2/2k]. \end{aligned} \quad (55)$$

The rest of this derivation follows exactly the ordinary spherical wave solution¹⁹ and will not be explicitly done here. The result is

$$\langle \chi_1 \chi_2 \rangle = 2\pi k^2 \int dz' \int d\mathbf{K} \Phi_n(\mathbf{K}, z') e^{i\mathbf{K} \cdot [\gamma(\mathbf{p}_1 - \mathbf{p}_2) + (1-\gamma)(\mathbf{p}_{02} - \mathbf{p}_{01})]} \sin^2[\gamma(z-z')K^2/2k], \quad (56)$$

where $\Phi_n(\mathbf{K}, z')$ is the three-dimensional turbulence spectrum. For the Kolmogorov spectrum, this is

$$\Phi_n(\mathbf{K}, z) = 0.033 C_n^2(z) K^{-11/3}. \quad (57)$$

Finite inner and outer scale effects can be included by using the modified von Karman spectrum

$$\Phi_n(\mathbf{K}, z) = 0.033 C_n^2(z) [K^2 + K_0^2]^{-11/6} \exp(-K^2/K_m^2), \quad (58)$$

where K_m is related to the inner scale, l_0 , by $K_m = 5.92/l_0$ and where K_0 is related to the outer scale, L_0 , by $K_0 = 2\pi/L_0$. Note that we have implicitly assumed that neither the inner nor outer scales vary with altitude.

¹⁹ Ishimaru, A. (1978) *Wave Propagation and Scattering in Random Media*, Vol. 2, Academic Press, N.Y.

The expression for the log amplitude covariance can be further simplified by using the fact that the turbulence spectrum depends only on the magnitude of K . Consider the integral:

$$I_2 = \int dK \Phi_n(K, z') e^{iK \cdot \rho_*} \sin^2[\gamma(z-z')K^2/2k], \quad (59)$$

where we have defined $\rho_* = \gamma(\rho_1 - \rho_2) + (1-\gamma)(\rho_{02} - \rho_{01})$. The vector K is a 2 dimensional vector in the plane transverse to the propagation direction. Let the direction of the vector ρ_* define the angular coordinate θ . We have

$$I_2 = \int d\theta \int K dK \Phi_n(K, z') e^{iK\rho_* \cos(\theta)} \sin^2[\gamma(z-z')K^2/2k] \quad (60)$$

$$= 2\pi \int K dK \Phi_n(K, z') J_0(K\rho_*) \sin^2[\gamma(z-z')K^2/2k]. \quad (61)$$

The log amplitude covariance is

$$\langle \chi_1 \chi_2 \rangle = 4\pi^2 k^2 \int dz' \int K dK \Phi_n(K, z') J_0(K|\gamma(\rho_1 - \rho_2) + (1-\gamma)(\rho_{02} - \rho_{01})|) \sin^2[\gamma(z-z')K^2/2k] \quad (62)$$

This expression can be simplified through the specification of the vector positions of the receivers and backscattering sources for the crossed path geometry. The receivers and sources are assumed to be symmetrically located about the origin of the transverse plane. Furthermore, it is assumed that the two sources and the two receivers are coplanar. Without loss of generality, we can define the sources and receivers to lie on the x axis. With reference to Figure 1, we have:

$$\begin{aligned} \rho_1 &= -\rho_2 \\ \rho_{01} &= -\rho_{02} \\ \rho_2 &= S/2 \\ \rho_{02} &= S_0/2. \end{aligned} \quad (63)$$

If we specify the turbulence spectrum as

$$\Phi_n(K, z) = C_n^2(z) \Phi_0(K), \quad (64)$$

we have

$$\langle \chi_1 \chi_2 \rangle = 4\pi^2 k^2 \int dz' C_n^2(z') \int K dK \Phi_0(K) J_0(K|\gamma S - (1-\gamma)S_0|) \sin^2[\gamma(1-\gamma)zK^2/2k] \quad (65)$$

$$= \int dz' C_n^2(z') W(z', z), \quad (66)$$

where the substitution $(z-z') = (1-\gamma)z$ has been made. W is the path weighting function defined by

$$W(z', z) = 4\pi^2 k^2 \int K dK \Phi_0(K) J_0(K|\gamma S - (1-\gamma)S_0|) \sin^2[\gamma(1-\gamma)zK^2/2k]. \quad (67)$$

The behavior of the weighting function can be inferred from the characteristics of the integrand. In Figure 2 the log amplitude spectrum, F , is plotted where

$$F(K) = 4\pi^2 k^2 K \Phi_0(K) \sin^2[\gamma(1-\gamma)zK^2/2k], \quad (68)$$

and $\Phi_0(K)$ is given by the modified von Karman spectrum. As is evident from the figure, the spectrum is insensitive to large scale sizes, a desirable feature of any scintillation-based effect. The \sin^2 term serves to attenuate the contributions from the large scale sizes. Also noteworthy is the broad peak in the inertial range, with a maximum approximately given by the first maximum of the \sin^2 , that is,

$$K_f = [\pi k / \gamma(1-\gamma)z]^{1/2} = 2\pi [2\lambda\gamma(1-\gamma)z]^{-1/2}. \quad (69)$$

This wavenumber corresponds to the Fresnel scale, l_f , for the spherical wave case. Using a wavelength of $0.5 \mu\text{m}$, this scale yields a numerical value of 5 cm for $z = 10 \text{ km}$, $z' = 5 \text{ km}$. Above this scale, the log amplitude spectrum is rapidly attenuated by the turbulence spectrum and the largest contribution to the spectrum comes from Fresnel scale turbulent eddies. A smaller contribution comes from larger scales in the inertial range, but there is negligible contribution from smaller scales. Above this scale the spectrum has very rapid oscillations due to the K^2 argument of the sine.

The crossed path effects enter via the J_0 term. Since the log amplitude spectrum is a positive quantity, it follows that the integral is a maximum when J_0 is a maximum, that is, when the argument of J_0 is zero. This condition is satisfied when

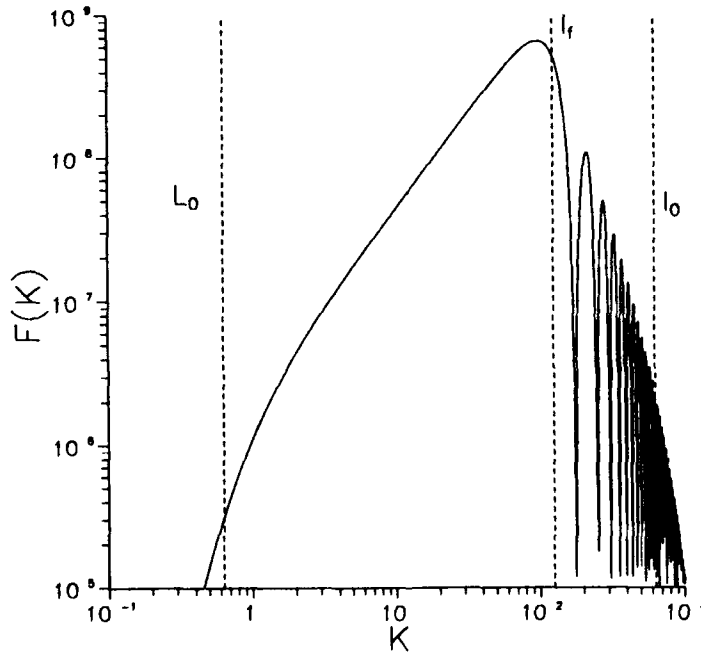


Figure 2. Log amplitude spectrum for the crossed path geometry. The spectrum is calculated using an outer scale L_0 of 10 m , an inner scale l_0 of 1 cm and $\lambda = 0.5 \mu\text{m}$. The backscattering altitude is 10 km and the point sources and point receivers are each separated by 1 m . The crossing altitude that results is 5 km and the corresponding value of the Fresnel scale l_f is 5 cm .

$$\gamma S = (1-\gamma)S_0, \quad (70)$$

or, solving for z' , the maximum is achieved when the path position, denoted by h , is given by

$$h = Sz/(S+S_0) = z/(1+S_0/S). \quad (71)$$

This expression is identical to the geometrical crossing altitude, as shown in Figure 1. The weighting function is a maximum at the crossing altitude; the geometrical theory and the more exact treatment agree. Note that the location of the peak depends only on the ratio of the receiver separation and backscatterer source separation. The crossing occurs at the path midpoint if these are equally separated.

The full weighting function is plotted in Figure 3 for backscattering from 10 km and equal source and receiver separation given by 1 meter. It should be emphasized that this is the point receiver and point backscatterer case. The weighting function is very sharply peaked at 5 km and appears to be negligible at less than 4.5 km and more than 5.5 km. In Figure 4, the vicinity of the peak is shown on an expanded scale and the absolute value of the weighting function is plotted. From this figure, it is clear that the weighting function has a $1/e$ width of the order of 175 meters. The weighting function also exhibits a very rapid decay; beyond about 300 m from the peak, the magnitude is down by nearly a factor of 100 or more, and beyond 800 m, it is down by about 1000 or more. This width does not depend solely on the ratio of the receiver to source separations, but also on their numerical values as well. It would be satisfying if the geometric width of the weighting function peak also agreed quantitatively with the exact theory. The weighting function width depends in a complex way on the first zeroes of the Bessel function and no simple analytical expression for the width can be obtained. A more thorough discussion of the resolution of the crossed path method is made after the theory is extended by the inclusion of finite source and receiver effects.

The approach of the crossed path technique can now be summarized. Utilizing our earlier results, it follows that

$$\begin{aligned} [4\langle I_1 \rangle \langle I_2 \rangle]^{-1} C_I(S) &= \langle \chi_1 \chi_2 \rangle \\ &= \int dz' C_n^2(z') W(z', z) \end{aligned} \quad (72)$$

The intensities are readily measured by photomultiplier tubes on the receivers. The average intensities and their covariance are statistically estimated from the time series of each receiver's intensity. The measurements of the average intensities and their covariance is equivalent to the measurement of a weighted average of C_n^2 along the path. These characteristics are not unique to the crossed path technique; the primary feature of the crossed path technique is the sharpness of its path weighting function. As our numerical example shows, backscattering from point sources at 10 km with 1 m separation with point detectors at 1 m separation gives a measurement of the weighted average of C_n^2 in a 175 m layer centered at 5 km.

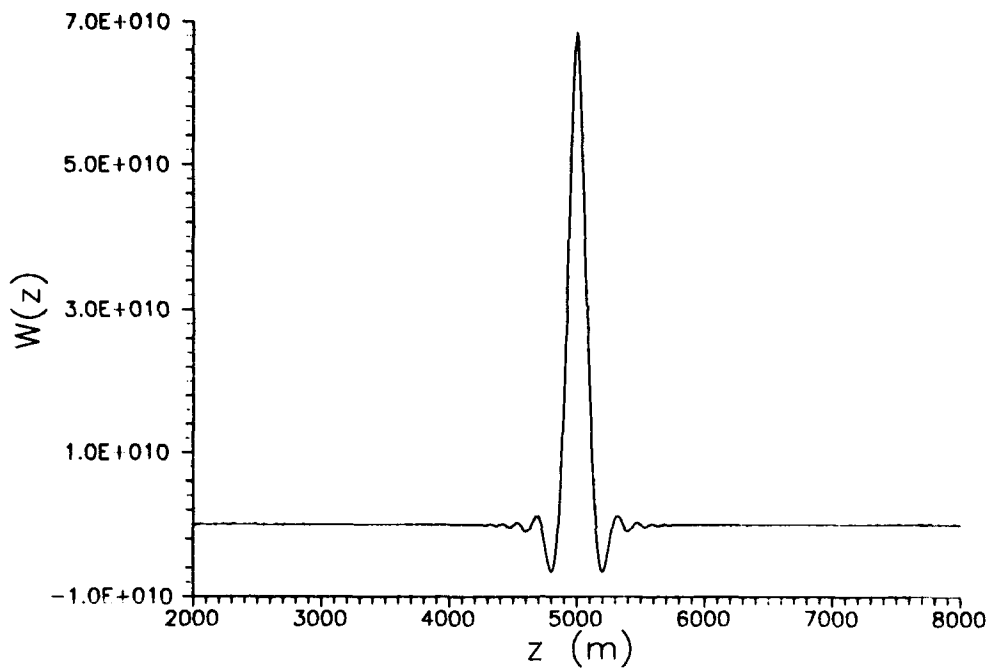


Figure 3. The crossed path weighting function versus altitude for point backscatterers and point receivers. The same numerical values as in Figure 2 are used.

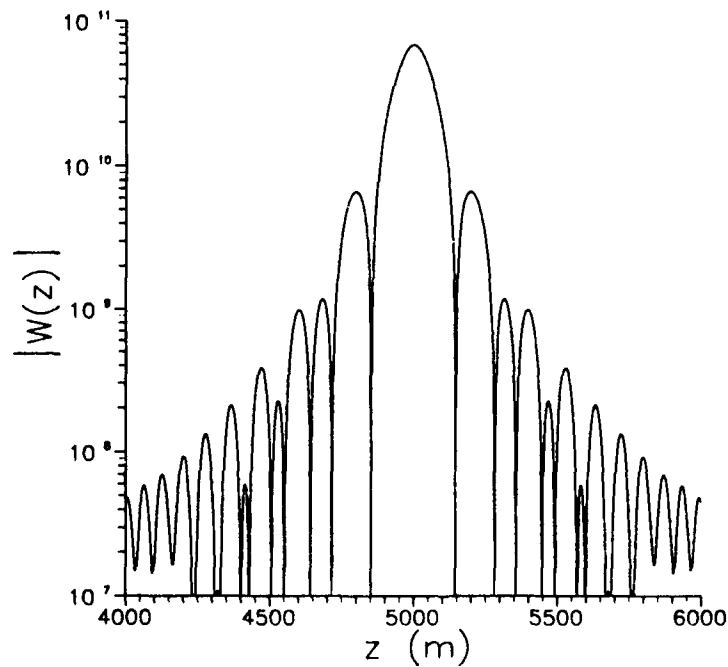


Figure 4. The absolute value of the weighting function is shown in the vicinity of the crossing altitude of 5 km. The same numerical values as in Figure 2 are used.

4.3 Finite Receiver and Source Effects

It is well known that scintillation effects are reduced by receiver aperture averaging. Intensity fluctuations are also less from an extended source than from a point source. The extension of the weighting function to include finite source and receiver effects is essential to the design and theory of a lidar C_n^2 measurement. First, the extension is made for the finite receiver effects. It is assumed that both receivers are identical, circular apertures of diameter D , or radius $R=D/2$. The measured quantity at each receiver is the integral of the intensity over the aperture

$$I_{T1} = \int I_1(x,y) dx dy, \quad (73)$$

where I_{T1} denotes the total intensity and an analogous expression holds for I_{T2} . This is related to the log amplitude by

$$\begin{aligned} I_{T1} &= \int I_{01}(x,y) e^{2\chi(x,y)} dx dy \\ &= I_{01} \int e^{2\chi(x,y)} dx dy, \end{aligned} \quad (74)$$

where we have assumed that the intensity in the absence of turbulence, I_{01} , is uniform across the aperture. Proceeding as before, we have that

$$\begin{aligned} \langle I_{T1} \rangle &= I_{01} \int \langle e^{2\chi(x,y)} \rangle dx dy \\ &= I_{01} \pi R^2 \langle e^{2\chi_1} \rangle, \end{aligned} \quad (75)$$

where the local homogeneity of χ has been used, that is, $\langle \chi(x,y) \rangle$ does not depend on (x,y) within the aperture and can be pulled out from the integral. The intensity covariance satisfies

$$\begin{aligned} C_{I_T}(S) &= \langle I_{T1} I_{T2} \rangle - \langle I_{T1} \rangle \langle I_{T2} \rangle \\ &= I_{01} I_{02} \iint dx dy dx' dy' \{ \langle e^{2[\chi_1(x,y) + \chi_2(x',y')]} \rangle - \langle e^{2\chi_1(x,y)} \rangle \langle e^{2\chi_2(x',y')} \rangle \}. \end{aligned} \quad (76)$$

Using the properties of the normal distribution, it follows that

$$\begin{aligned} C_{I_T}(S) &= [\langle I_{T1} \rangle \langle I_{T2} \rangle / (\pi R^2)^2] \iint dx dy dx' dy' \{ e^{4C_\chi(x-x', y-y')} - 1 \} \\ &\approx [\langle I_{T1} \rangle \langle I_{T2} \rangle / (\pi R^2)^2] \iint dx dy dx' dy' 4 C_\chi(x-x', y-y'). \end{aligned} \quad (77)$$

Since $C_\chi = \langle \chi_1 \chi_2 \rangle$, it is clear that the critical quantity consists of the integral of $\langle \chi_1 \chi_2 \rangle$ over the apertures. This is denoted by $\langle \chi_1 \chi_2 \rangle_T$ and is given by

$$\langle \chi_1 \chi_2 \rangle_T = (\pi R^2)^{-2} \iint dx dy dx' dy' \langle \chi_1(x,y) \chi_2(x',y') \rangle. \quad (78)$$

Note that it is normalized by the square of the receiver area. Interchanging the order of ensemble averaging and integration gives

$$\langle \chi_1 \chi_2 \rangle_T = (\pi R^2)^{-2} \left\langle \left[\int dx dy \chi_1(x, y) \right] \left[\int dx' dy' \chi_2(x', y') \right] \right\rangle. \quad (79)$$

The problem is reduced to evaluating the integrated log amplitude at the apertures. Call these quantities χ_{1T} and χ_{2T} for the two receivers. These are given by the forms

$$\chi_{1T} = (\pi R^2)^{-1} \int dx dy \chi_1(x, y), \quad (80)$$

where the integral is over a circle of diameter D centered at the transverse vector \mathbf{p}_1 . Substituting for χ_1 from our earlier results produces

$$\chi_{1T}(\mathbf{r}_1) = k/(\pi R^2) \int d\mathbf{p}_r \int dz' \int dv(\mathbf{K}, z') e^{i\mathbf{K} \cdot [\gamma(\mathbf{p}_1 + \mathbf{p}_r) + (1-\gamma)\mathbf{p}_{02}]} \sin[\gamma(1-\gamma)zK^2/2k]. \quad (81)$$

The integral over \mathbf{p}_r inside the aperture can be evaluated. Consider the integral

$$I_3 = \int d\mathbf{p}_r e^{i\mathbf{K} \cdot \gamma \mathbf{p}_r}. \quad (82)$$

Converting from a vector integral to an integral over angle and the magnitude of ρ produces

$$\begin{aligned} I_3 &= 2\pi \int \rho_r d\rho_r J_0(K\gamma\rho_r) \\ &= 2\pi R^2 \left[\frac{J_1(K\gamma R)}{(K\gamma R)} \right] \end{aligned} \quad (83)$$

where the integral has been evaluated using a property of Bessel functions. The effect of the receiver aperture averaging is to include a further term in the integrand that behaves as $J_1(K\gamma R)/(K\gamma R)$. Using this result in our expression for χ_{1T} , we get

$$\chi_{1T} = 2k \int dz' \int dv(\mathbf{K}, z') e^{i\mathbf{K} \cdot [\gamma \mathbf{p}_1 + (1-\gamma)\mathbf{p}_{02}]} \left[\frac{J_1(K\gamma R)}{(K\gamma R)} \right] \sin[\gamma(1-\gamma)zK^2/2k]. \quad (84)$$

Note that the scaling by the receiver area πR^2 has been cancelled out by our normalization. In the following we will drop the subscript T on $\langle \chi_1 \chi_2 \rangle$. The derivation of $\langle \chi_1 \chi_2 \rangle$ proceeds exactly as before with the inclusion of this additional term in the integrand and the result is

$$\langle \chi_1 \chi_2 \rangle = 16\pi^2 k^2 \int dz' C_n^2(z') \int K dK \Phi_0(K) J_0(K\gamma S - (1-\gamma)S_0) \sin^2[\gamma(1-\gamma)zK^2/2k] \left[\frac{J_1(K\gamma R)}{(K\gamma R)} \right]^2. \quad (85)$$

This in turn defines a new path weighting function by

$$W(z', z) = 16\pi^2 k^2 \int K dK \Phi_0(K) J_0(K\gamma S - (1-\gamma)S_0) \sin^2[\gamma(1-\gamma)zK^2/2k] \left[\frac{J_1(K\gamma R)}{(K\gamma R)} \right]^2. \quad (86)$$

The $J_1(x)/x$ term in the integrand acts as a low pass filter. Spatial wavenumbers satisfying $K \gg 1/(\gamma R)$ are attenuated. The receiver aperture averaging reduces the scintillation and the covariance by filtering or averaging out the contributions from scale sizes smaller than the aperture. A more precise criterion can be stated using the $1/e$ point of $[J_1(x)/x]^2$. This value, 1.9, is used to define the *passband of the filter*. Specifically, wavenumbers less than $1.9/\gamma R$ will not be attenuated or reduced by aperture averaging.

The receiver aperture averaging is a critical system parameter. A larger aperture is desirable, as it increases the total signal received. It cannot be so large as to significantly reduce the scintilla-

tion. These two criteria can be satisfied if the Fresnel scale eddies are within the passband. Specifically, we require

$$2\pi [2\lambda\gamma(1-\gamma)z]^{-1/2} \leq (1.9)/\gamma R \quad (87)$$

be satisfied for the altitude, z' , where the weighting function is peaked. Additional attenuation at altitudes not in the weighting function peak does not matter. Alternatively, this equation can be inverted to impose the requirement that the aperture radius, R , must satisfy

$$R \leq (1.9/2\pi\gamma) [2\lambda\gamma(1-\gamma)z]^{1/2}. \quad (88)$$

In practice, the backscattering will not be from a point but from an area with non-zero cross sectional area determined by the lidar beam width at the scattering altitude. The beam may wander and be broadened due to the turbulence on the uplink. These phase effects will be discussed subsequently. Here, the scintillation effects of the uplink are considered. The lidar beam at the backscatter altitude is assumed to have a diameter d (or radius $a = d/2$). The scintillation on the lidar beam results in a fine scale speckle pattern of intensity within a circle of radius a . The intensity is not uniform within the circle of radius a , but rather there are intensity hot spots of the size given by the Fresnel scale. If the averaging time is longer than the wind clearing time for the largest Fresnel scale hot spots, the speckle structure of the light incident on the backscattering region can be ignored and the backscattering region can be assumed to be uniformly illuminated. This criteria can be more precisely stated. The lidar beam is assumed to be collimated and locally approximated by a plane wavefront. If V is the wind speed transverse to the beam at z , the scattering altitude, the averaging time T must satisfy

$$T > (\lambda z)^{1/2}/V, \quad (89)$$

where the plane wave Fresnel scale has been used. For a $0.5 \mu\text{m}$ beam at 10 km, this requires that the time be longer than 0.07 sec for a 1 m/s wind and 7 msec for a 10 m/s wind. These criteria are easily satisfied.

The illumination of the backscatterers can be regarded as uniform. In addition, the scattering process is either Rayleigh scattering from air molecules or Mie scattering from aerosols. In either case, the scattering process is incoherent. The net result is that the backscattering of an incident beam of radius a can be treated as a uniform, incoherent source of radius a . The details of this calculation are straightforward but tedious. Let $I(x,y,r)$ be the intensity observed at (x,y,z) from a point source located at vector position r in the $z = 0$ plane. For an incoherent source, observed at (x,y,z) , the total intensity I_T is given by the incoherent superposition of point sources:

$$I_T = \int I(x,y,r) dr, \quad (90)$$

where the integration is over the source distribution volume. The same steps as for receiver aperture averaging are followed to derive the effect of the finite source. The net result is the inclusion of an additional term in the integrand for the log amplitude covariance, a term given by

$$4 \left[\frac{J_1(K(1-\gamma)a)}{K(1-\gamma)a} \right]^2. \quad (91)$$

The resulting log amplitude covariance, incorporating the effects of finite receiver and source, is thus

$$\langle \chi_1 \chi_2 \rangle = 64\pi^2 k^2 \int dz' C_n^2(z') \int K dK \Phi_0(K) J_0(K\gamma S - (1-\gamma)S_0) \left[\frac{J_1(K(1-\gamma)a)}{K(1-\gamma)a} \right]^2 \left[\frac{J_1(K\gamma R)}{K\gamma R} \right]^2 \sin^2[\gamma(1-\gamma)zK^2/2k]. \quad (92)$$

This defines the overall path weighting function by

$$W(z', z) = 64\pi^2 k^2 \int K dK \Phi_0(K) J_0(K\gamma S - (1-\gamma)S_0) \left[\frac{J_1(K(1-\gamma)a)}{K(1-\gamma)a} \right]^2 \left[\frac{J_1(K\gamma R)}{K\gamma R} \right]^2 \sin^2[\gamma(1-\gamma)zK^2/2k]. \quad (93)$$

The effect of a source of radius a is the same as that of a receiver of the same radius, but with γ replaced by $1-\gamma$. The finite extent of the source results in filtering of the spatial scales contributing to the scintillation spectrum and thereby reduces the scintillation. In order to keep this reduction to a minimum, we again consider the $1/e$ point of the $[J_1(x)/x]^2$ term. This provides the specific criterion that

$$2\pi [2\lambda\gamma(1-\gamma)z]^{-1/2} \leq (1.9)/(1-\gamma)a \quad (94)$$

be satisfied for all altitudes of interest. The requirement for the backscatter spot size is

$$a \leq 1.9/[2\pi(1-\gamma)] [2\lambda\gamma(1-\gamma)z]^{1/2}. \quad (95)$$

The following examples are treated to provide some feel for the numerical constraints on the receiver and backscatter spot size. The laser wavelength is assumed to be $0.5 \mu\text{m}$, the backscatter spot at 10 km, and the crossing altitude is 5 km. In this case neither the lidar spot at 10 km nor the receiver radius can exceed approximately 3 cm without reduction in scintillation. It can be seen that the allowable sizes increase as the square root of the backscatter altitude. For a 2 km backscatterer and a crossing altitude of 1 km, the limiting size is about 1 cm. These are tight restrictions. In Figure 5, the behavior of the weighting function in the vicinity of the peak is shown for various aperture sizes for the usual numerical example. It can be seen that the effect of aperture averaging is to cause both a decrease in the magnitude and an increase in the width of the peak. The signal strength and resolution are degraded.

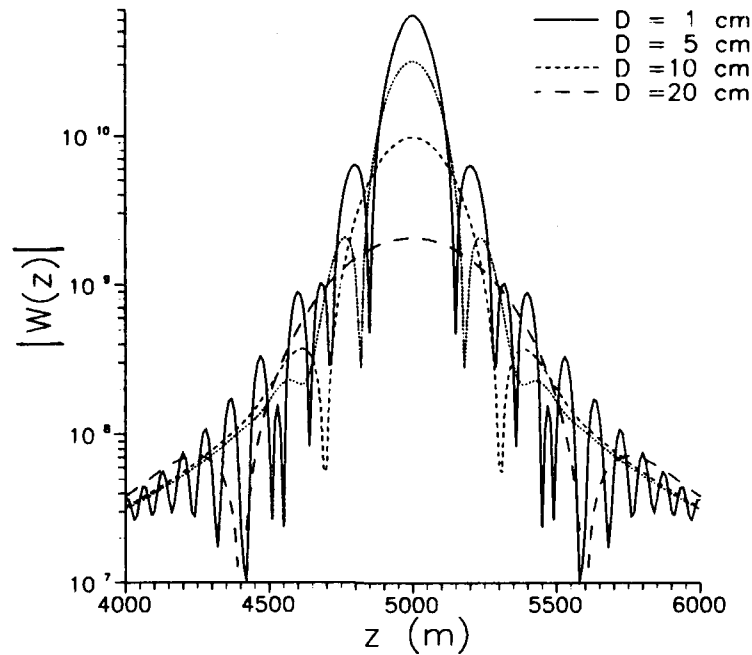


Figure 5. The absolute value of the weighting function is shown in the vicinity of the crossing altitude of 5 km for several values of aperture diameters. The same numerical values as in Figure 2 are used, except that the receiver and backscatter diameters are assumed equal and given by the values shown. Note that the excursions to small values shown in Figure 4 are absent in the present figure. This absence is a numerical artifact of the larger step size in z used in the calculation.

4.4 Inner Scale Effects

In the theory, one scale size has emerged that is of critical importance: the Fresnel scale. However, the presentation has oversimplified one aspect of the problem; namely, we have assumed that the inner scale of turbulence is 1 cm, a value less than the Fresnel scale in the calculations presented. In practice, the inner scale is not a constant, but is itself a function of both altitude and turbulence strength. The distinction between the inner scale for velocity and temperature fluctuations must be made in discussing inner scale. In all that follows, we will assume the inner scale for temperature fluctuations. The inner scale for temperature, and hence refractive index, fluctuations is defined by²⁰

$$l_0 = 7.4 (D^3/\epsilon)^{1/4}, \quad (96)$$

²⁰Hill, R.J., and Clifford, S.F. (1978) Modified spectrum of atmospheric temperature fluctuations and its application to optical propagation, *J. Opt. Soc. Am.*, 68:892-899.

where D is the diffusion coefficient and ϵ is the eddy dissipation rate. Values for l_0 have been reported as millimeters²¹ in the first few meters above the surface, centimeters in the first few hundred meters and in the troposphere²² and tens of centimeters in the stratosphere²³.

In Figure 6, the value of the weighting function is shown as a function of l_0 for different receiver and source diameters. The value of the weighting function is plotted at the crossing altitude (for the $S = S_0$ case) where the weighting function is a maximum. The dependence on inner scale is computed via the modified von Karman spectrum. The crossing altitude is again 5 km and yields a Fresnel scale of approximately 5 cm. As is evident from the figure, the value of the weighting function does not depend on inner scale provided l_0 is smaller than the Fresnel scale. (The effect of inner scale has a lesser dependence on source and receiver diameters.) If the Fresnel scale is smaller than the inner scale, the refractive index spectrum dominates the integrand of the weighting function at the small scale sizes of the inertial range, with a negligible contribution from the \sin^2 term. The inner scale is then the critical parameter instead of the Fresnel scale.

In Figure 7, the effect of inner scale on the weighting function in the vicinity of the crossing altitude is shown. Besides the suppression of the magnitude of the peak value, it is seen that there is also a significant broadening of the weighting function when l_0 is greater than the Fresnel scale. The width of the weighting function is increased and hence the resolution of the crossed path technique is degraded.

The contribution of inner scale effects to intensity variance and covariance has been noted before²⁰ for propagation through homogeneous turbulence (that is, where C_n^2 is a constant along the path). Its effect in the crossed path technique is to be expected, but has not been mentioned in any of the previous works on the variants of the crossed path technique^{7,12,19,24,25,26,27}. Indeed, it appears that the effect of inner scale discussed here also applies to the techniques based on binary star data; it is a consequence of the covariance of log amplitude. The contribution of the inner scale in a crossed path lidar system must be eliminated or reduced if a meaningful measurement of C_n^2 is to be made; if it is not, the measurement depends on two unknown parameters, l_0 and C_n^2 . The situation is mitigated somewhat by a relation between ϵ and C_n^2 . Specifically, it can be shown that

²¹Hill, R.J. (1983) Inner-scale effect on the irradiance of light propagating in atmospheric turbulence, in *Laser Beam Propagation in the Atmosphere. Proc. of the SPIE*, 410.

²²Hocking, W.K. (1985) Measurement of turbulent energy dissipation rates in the middle atmosphere by radar techniques: A review, *Radio Sci.*, 20:1403-1422.

²³Barat, J. (1982) Some Characteristics of Clear-Air Turbulence in the Middle Stratosphere, *J. Atmos. Sci.*, 39:2553-2564.

²⁴Lee, R.E., and Harp, J.C. (1969) Weak Scattering in Random Media, with Applications to Remote Probing, *Proc. IEEE*, 57:375-406.

²⁵Roddiar, C., and Vernin, J. (1977) Relative contribution of upper and lower atmosphere to integrated refractive-index profiles, *Appl. Opt.*, 16: 2252-2256.

²⁶Rocca, A., Roddiar, F., and Vernin, J. (1974) Detection of atmospheric turbulence layers by spatiotemporal and spatioangular correlation measurements of stellar-light scintillation, *J. Opt. Soc. Am.*, 64:1000-1004.

²⁷Azouit, M., and Vernin, J. (1980) Remote Investigation of Tropospheric Turbulence by Two-Dimensional Analysis of Stellar Scintillation, *J. Atmos. Sci.*, 37:1550-1557.

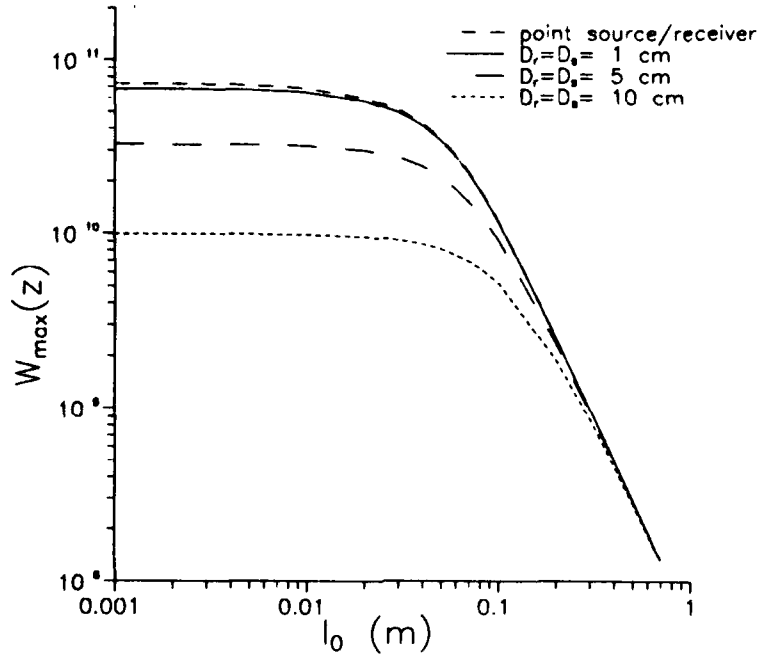


Figure 6. The maximum value of the weighting function is shown versus the inner scale, l_0 . The calculations were made using the modified von Karman spectrum. The source and receiver diameters were assumed equal and given by the values shown. The source was located at 10 km, giving the crossing altitude and weighting function maximum at 5 km. The other values are identical to those used in Figure 2.

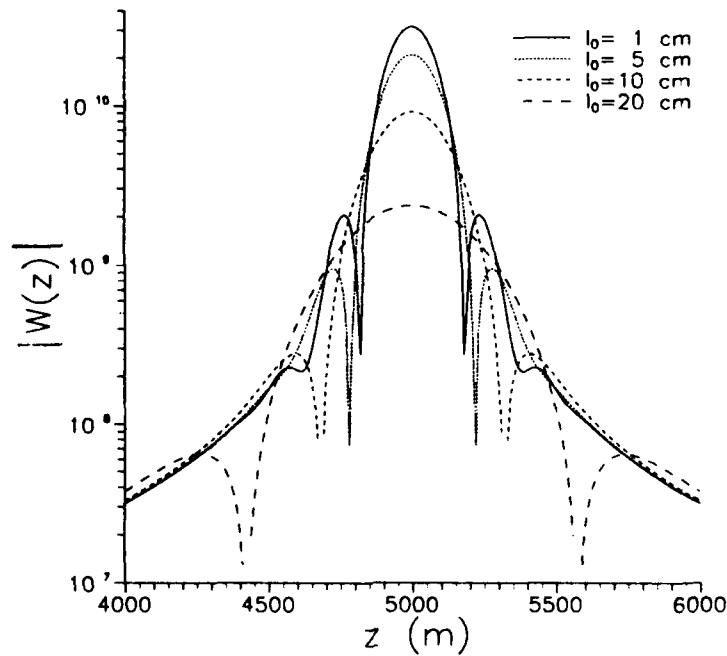


Figure 7. The absolute value of the weighting function is shown in the vicinity of the crossing altitude of 5 km for several values of inner scale, l_0 . The same numerical values as in Figure 2 are used, except that the receiver and backscatterer diameters are assumed equal and given as 5 cm.

$$C_n^2 = \alpha \epsilon^{2/3} f(T, P, dT/dz), \quad (97)$$

where α is a constant of order unity and f is a function of meteorological (that is, non-fluctuating) parameters. Upon substitution of l_0 , it follows that

$$C_n^2 = \alpha(7.4)^{8/3} D^2 f(T, P, dT/dz) l_0^{-8/3}. \quad (99)$$

Thus, C_n^2 is inversely related to l_0 ; large C_n^2 means small l_0 . We have also seen that for small l_0 , the Fresnel scale effects dominate and the weighting function depends very little on the inner scale. Strong layers of turbulence are likely to have small l_0 (of the order of centimeters or less) in the boundary layer and troposphere and the weighting function can be unambiguously calculated for these cases. For weak layers, the weighting function depends on the unknown l_0 . If the inner scale is assumed to be less than the Fresnel scale for all altitudes of interest, the effect is to overestimate the weighting function for weak layers, and thereby underestimate C_n^2 . As can be seen from Figure 6, the averaging effect of the finite sources and receivers tends to reduce the overestimation of the peak of the weighting function.

This effect of inner scale cannot be eliminated and appears to impose a fundamental limitation on the crossed path method. The exact contribution of inner scale is unknown; the calculations performed above have established that there is a contribution, but these calculations have been based on the von Karman spectrum. This spectrum is ad hoc, without experimental basis, and was introduced by Tatarskii¹⁶ for mathematical convenience. It does not model the experimentally observed bump in the temperature spectrum²⁰. Calculations performed by Hill²⁸ for a point source and point detector show for propagation through homogeneous turbulence that the intensity variance has a significant contribution from the inner scale region that is manifested for l_0 greater than approximately $0.5(\lambda z)^{1/2}$. Hill's analysis may be interpreted as showing that the modified von Karman spectrum is a reasonable approximation to the true spectrum for l_0 greater than about $3(\lambda z)^{1/2}$. For the region $0.2(\lambda z)^{1/2}$ to $2(\lambda z)^{1/2}$, the agreement is poor due to the "bump" and the modified von Karman spectrum underestimates the spectrum. A further interpretation of Hill's analysis is that it provides evidence that the effect of inner scale may be more prominent than the effect predicted by using the modified von Karman spectrum.

The criterion for the inner scale effects to be negligible is that the Fresnel scale be larger than l_0 , or specifically,

$$l_0 < [2\lambda\gamma(1-\gamma)z\lambda']^{1/2}, \quad (99)$$

where z is the altitude of the backscattering. The contribution of the inner scale of the spectrum to the crossed path covariance may be minimized by maximizing the Fresnel scale. It is easy to see that the Fresnel scale is maximized for $\gamma = 1/2$, when the crossing occurs at the path midpoint. This is equivalent to the requirement that the receiver and source separations be equal. This provides a strong motivation for choosing the midpoint as the crossing point.

Finally, it is worth noting that, in the limit $z \gg z'$, the above requirement then becomes

$$l_0 < (2\lambda z')^{1/2}. \quad (100)$$

²⁸Hill, R.J. (1988) Comparison of scintillation methods for measuring the inner scale of turbulence, *Appl. Opt.*, 47:2187-2193.

The altitude of interest is now the crossing altitude, z' , rather than the source altitude. This is the situation with the binary star method. Inner scale effects should manifest themselves in the binary star data.

It can be argued that the spatial filtering performed by the finite receiver or source sizes can be used to filter out the inner scale effect on the covariance. In principle it is possible to reduce these effects by the use of a large enough aperture, as can be seen from Figure 6. The effect will be reduced if the aperture sizes are selected such that the spatial wavenumbers in the band $(2\pi/l_0, K_f)$ are attenuated. If a maximum allowable inner scale is chosen as 10 cm and equal source and receiver separations are assumed, the filtering of these effects requires receiver and source sizes greater than about 12 cm in diameter. A practical lidar system could readily meet this criteria, but the tradeoff is a reduction in signal strength and resolution. In addition, the filtering provided by $J_1(x)/x$ is gradual and does not have a sharp transition; therefore, the inner scale effect is not eliminated, but rather reduced. The apertures would have to be much larger to get a significant reduction, but this would yield a significant reduction in scintillation.

4.5 Overall Path Weighting Function

The complication that results when both sources are in both receiver fields of view was discussed in Section 4.1 in terms of intensity. The weighting function described so far has applied to the crossed path term. The theory can be extended to include the effect of the other three terms to yield an overall path weighting function. Equation (34) gives the intensity covariance between receivers 1 and 2:

$$C_I(S) = [\langle I_{11}I_{21} \rangle - \langle I_{11} \rangle \langle I_{21} \rangle] + [\langle I_{12}I_{22} \rangle - \langle I_{12} \rangle \langle I_{22} \rangle] + [\langle I_{12}I_{21} \rangle - \langle I_{12} \rangle \langle I_{21} \rangle] + [\langle I_{11}I_{22} \rangle - \langle I_{11} \rangle \langle I_{22} \rangle], \quad (101)$$

where I_{ij} is the j^{th} source at the i^{th} receiver. The formal expression for the log amplitude covariance, Equation (62), is in fact very general and states the covariance in terms of arbitrary 2-dimensional vectors for receiver positions \mathbf{p}_1 and \mathbf{p}_2 and for source positions \mathbf{p}_{01} and \mathbf{p}_{02} . The first and second terms of the total intensity covariance will yield a path weighting function found by setting $\mathbf{p}_{01} = \mathbf{p}_{02}$, that is, both sources collocated:

$$W_{11,21}(z',z) = W_{12,22}(z',z) = 64\pi^2 k^2 \int K dK \Phi_0(K) J_0(K\gamma S) \left[\frac{J_1(K(1-\gamma)a)}{K(1-\gamma)a} \right]^2 \left[\frac{J_1(K\gamma R)}{K\gamma R} \right]^2 \sin^2[\gamma(1-\gamma)zK^2/2k], \quad (102)$$

where the subscripts on W denote the particular covariance term that gives rise to the effect. This path weighting represents the intensity covariance of a single source viewed by two receivers separated by S . The third term is simply the crossed path term. In our current notation, this term is:

$$W_{12,21}(z',z) = 64\pi^2 k^2 \int K dK \Phi_0(K) J_0(K\gamma S - (1-\gamma)S_0) \left[\frac{J_1(K(1-\gamma)a)}{K(1-\gamma)a} \right]^2 \left[\frac{J_1(K\gamma R)}{K\gamma R} \right]^2 \sin^2[\gamma(1-\gamma)zK^2/2k]. \quad (103)$$

The last term is given by the uncrossed path, which we get by setting $\rho_{01} = -\rho_{02}$, with $\rho_{01} = S_0/2$ (note sign reversal from crossed path case):

$$W_{11,22}(z',z) = 64\pi^2 k^2 \int K dK \Phi_0(K) J_0(K\gamma S + (1-\gamma)S_0) \left[\frac{J_1(K(1-\gamma)a)}{K(1-\gamma)a} \right]^2 \left[\frac{J_1(K\gamma R)}{K\gamma R} \right]^2 \sin^2[\gamma(1-\gamma)zK^2/2k]. \quad (104)$$

It will be assumed that the average of source 1 is the same as source 2 in either receiver 1 or 2. Specifically, we assume that

$$\langle I_{11} \rangle = \langle I_{21} \rangle = \langle I_{12} \rangle = \langle I_{22} \rangle. \quad (105)$$

This results in the simple addition of the individual path weighting functions to yield the overall path weighting function given by

$$W(z',z) = 64\pi^2 k^2 \int K dK \Phi_0(K) \left[2J_0(K\gamma S) + J_0(K\gamma S - (1-\gamma)S_0) + J_0(K\gamma S + (1-\gamma)S_0) \right] \left[\frac{J_1(K(1-\gamma)a)}{K(1-\gamma)a} \right]^2 \left[\frac{J_1(K\gamma R)}{K\gamma R} \right]^2 \sin^2[\gamma(1-\gamma)zK^2/2k] \quad (106)$$

The net effect of both sources being seen by both receivers is the inclusion of additional J_0 terms in the integrand. In Figures 8 and 9, the overall weighting function is shown for comparison with the crossed term for separations of 10 and 1 cm, respectively. The overall weighting function for the 1 cm case is significantly different than the cross term only. For the 10 cm separation, the weighting function at the peak is unaffected by the additional terms. These results have a simple, physical interpretation that substantiates the qualitative argument presented in Section 4.1. The relevant Fresnel scale for the 1 km backscattering with midpoint crossing is about 1.6 cm (for $\lambda = 0.5 \mu\text{m}$) corresponding to the peak in the log amplitude spectrum (since this is larger than the inner scale of 1 cm). First, consider the contribution of the term $J_0(K\gamma S)$. If x_0 is the first zero of J_0 , there will be minimal contribution to the integral over K for values satisfying

$$K > x_0/\gamma S. \quad (107)$$

Writing this in terms of scale sizes, there will be minimal contribution for scale sizes, l_1 , satisfying

$$l_1 < 2\pi\gamma S/x_0. \quad (108)$$

Substitution of the values into the right hand side for the peak altitude gives 1.3 cm and 13 cm for 1 cm and 10 cm separations, respectively. The spectral peak at the Fresnel scale is within the "passband" of the J_0 term for the 1 cm separation, while it is not for the 13 cm case. The J_0 term that arises from the overall path scintillation of each source contributes when the source separation is within a Fresnel scale and does not contribute significantly at larger separation. Note

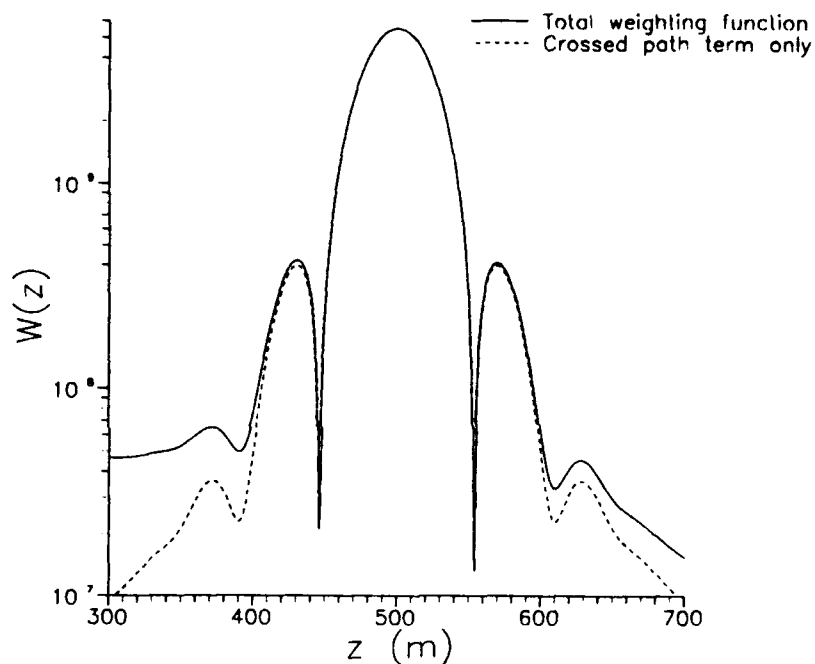


Figure 8. The absolute value of the weighting function is shown in the vicinity of the crossing altitude of 500 m showing the magnitude of the total function and the crossed term only. The calculation is done for 1 km backscattering, inner scale of 1 cm, source and receiver separations equal and given by 10 cm, and source and receiver apertures of 1 cm.

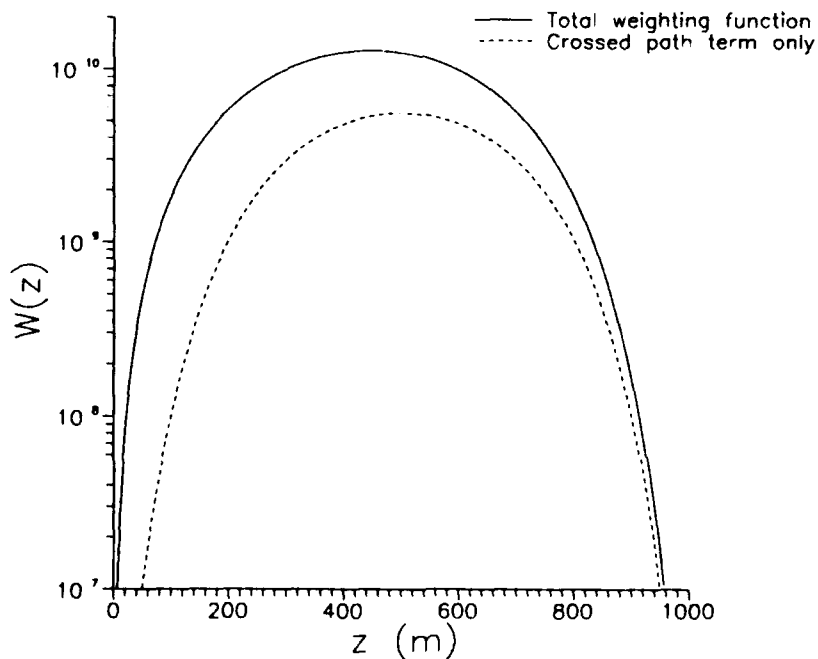


Figure 9. The absolute value of the weighting function is shown in the vicinity of the crossing altitude of 500 m showing the magnitude of the total function and the crossed term only. The calculation is done using the same numerical values as Figure 8, except the source and receiver separations are given by 1 cm.

that this numerical comparison has been made for the value at the peak corresponding to the crossing altitude. Despite the negligible contribution at the peak for the 10 cm case, the figure shows that for other altitudes, the contribution from the uncrossed terms may be larger than that from the crossed term, but these are less important since the weighting function is down by more than an order of magnitude from its peak value. The contribution of the $J_0(K\gamma S)$ term is not symmetric about the midpoint, but applies more weight to the receiver end of the path.

Similar arguments apply to the second uncrossed term, $J_0(K\gamma S + (1-\gamma)S_0)$. There will be negligible contribution from this term from scales satisfying

$$l_2 < 2\pi[\gamma S + (1-\gamma)S_0]/x_0. \quad (109)$$

Comparing this with the magnitude of the term from the single source, whole path scintillation, it can be seen that $l_1 < l_2$ for any values of S , S_0 , and γ . From this inequality, it follows that this second uncrossed term has a narrower passband and thus a smaller contribution than the single source uncrossed term. In our specific numerical example, the values of l_2 are 2.6 cm and 26 cm respectively for 1 and 10 cm separations. Both these values are larger than the Fresnel scale and thus in both cases there are negligible contributions of this term to the total weighting function.

This discussion has been more quantitative than the earlier arguments about the importance of the uncrossed path terms to the overall weighting function, but the conclusions have been the same. The earlier discussion argued that the uncrossed covariances were negligible with respect to their uncrossed variances, while in this section it has been shown that they may also be negligible with respect to the crossed covariance. For a lidar system, the separations are likely to be tens of centimeters or even meters and these numbers yield cutoff scale sizes for the uncrossed term that are larger than the Fresnel scale. Consequently, their contribution to the overall weighting function is negligible. This is not true for the binary star approach. Indeed, the numerical example of a 1 cm separation at 1 km is equivalent (or 10 cm at 10 km) to an angular separation of the sources of 10 μ rad. This is the separation corresponding to the double star Castor which has been used in the binary star method²⁶.

4.6 Uplink Propagation Effects

A critical requirement of a lidar-based technique that has not been addressed is the effect of the uplink propagation, or more precisely, the effect of the propagation of the lidar beam from the transmitter to the backscattering region. Aspects of this problem have been mentioned in the discussion of the effect of backscatter spot size. It was argued that the scintillation effect on the uplink would not be a problem because of the statistical averaging requirements. With respect to beam size, a very strict criterion was presented in terms of the relevant Fresnel scale: for a 10 km backscatter, the (0.5 μ m) beam should be less than 6 cm in diameter, while for 1 km backscatter, it should be less than 2 cm.

This criterion needs to be examined in terms of the specific effects of beam broadening due to diffraction, turbulence and beam wander. The average beam width, ρ_b , for a beam of diameter D , can be expressed in terms of the diffraction-related width, ρ_d , and the turbulence-related width, ρ_t , by

$$\langle \rho_b^2 \rangle = (D/2)^2 [1 - z/f]^2 + \rho_d^2 + \langle \rho_t^2 \rangle, \quad (110)$$

where f is the distance to the focus (for a collimated beam, $f = \infty$) and where the diffraction width is given by

$$\rho_d = 2z/(kD). \quad (111)$$

The turbulence term is written as²⁹

$$\begin{aligned} \langle \rho_t^2 \rangle &= 4z^2/(k\rho_0)^2 \left[1 - 0.62(\rho_0/D)^{1/3} \right]^{6/5} \\ &= \rho_d^2 (D/\rho_0)^2 \left[1 - 0.62(\rho_0/D)^{1/3} \right]^{6/5}, \end{aligned} \quad (112)$$

where ρ_0 is the transverse coherence length³⁰ for propagation from 0 to z given by

$$\rho_0 = (1.46 k^2 \int_0^z C_n^2(\eta) (1 - \eta/z)^{5/3} d\eta)^{-3/5}. \quad (113)$$

The transverse coherence length ρ_0 is simply related to the atmospheric coherence length³¹ r_0 by $r_0 = 2.1 \rho_0$. This expression is the spherical wave form of the transverse coherence length; some authors⁹ use the plane wave form of ρ_0 for a collimated beam which has no altitude weighting in the integrand. In the turbulence literature, this beam broadening is usually discussed in terms of the short-term beam width or the tilt-corrected beam width; the long-term beam width includes the turbulence beam wander. Measurements of r_0 for the plane wave case yield typical values at 0.5 μm of from 5 to 10 cm, with higher values at astronomical sites. These values translate into a range for ρ_0 of about 2.5 to 5 cm. The broadening of a 0.5 μm beam can be estimated at 1 km and at 10 km using the value of 2.5 cm for ρ_0 . This requires the assumption that ρ_0 is the same for these cases as for the ground to space case. This is reasonable since generally the largest turbulence occurs near the ground and in the boundary layer and dominates ρ_0 . For a collimated beam of 2 cm diameter at the transmitter, the turbulence beam broadening will be much smaller than the diffraction effect: the 2 cm diameter beam will be of the order of 2.6 cm diameter at 1 km and 17.4 cm in diameter at 10 km. For a focused beam, the 2 cm transmitter has a spot size of 1.9 cm if focused at 1 km and 17.2 cm if focused at 10 km. A 5 cm transmitter produces an interesting example where both turbulence and diffraction effects contribute: at 10 km, the collimated and focused cases yield spot sizes of 11.6 and 10.6 cm, respectively. If the 5 cm transmitter is focused at 1 km, the spot size is 1.06 cm, while the collimated case yields 5.1 cm. The spread due to diffraction can be reduced by increasing the aperture, but the turbulence spread remains and is asymptotically independent of the diameter.

These calculations demonstrate that beam spreading is an important issue in the crossed path technique. For a collimated beam, the narrow beam widths required to meet the specifications for the spot size result in diffraction broadening being the dominant effect. If a focused beam is used instead with a larger transmitter diameter, turbulence broadening becomes the dominant effect in

²⁹Fante, R.L. (1975) Electromagnetic Beam Propagation in a Turbulent Media, *Proc. IEEE*, 63: 1669-1692.

³⁰Yura, H.T. (1971) Atmospheric Turbulence Induced Laser Beam Spread, *Appl. Opt.*, 10:2771-2773.

³¹Fried, D.L. (1966) Optical Resolution Through a Randomly Inhomogeneous Medium, *J. Opt. Soc. Am.*, 56:1372-1379.

determining spot size. When turbulence dominates, it should be emphasized that the beam width is a fluctuating quantity, even during "homogeneous" turbulence conditions, and the width is specified above in terms of its ensemble value. Physically, the effect of beam spread is to reduce the peak value of the weighting function and broaden its width. The effect of the fluctuating lidar spot size is that now the weighting function itself is a fluctuating quantity. The relevant quantity is the average weighting function. This in turn requires that the transverse coherence length be known, or equivalently, the C_n^2 profile.

The calculation of the average weighting function needs to be done numerically. This calculation will not be performed here and is left for follow-on research. Certain aspects of the average can be estimated, however. The situation is not as significant for the crossed path approach as it may seem. As can be seen from Figure 5, even for a very broadened beam of 20 cm, the weighting function is still very narrow and far superior to other techniques. Furthermore, the small spots have a weighting function with the greatest magnitude, while for large spots, the weighting function is the smallest. Whatever the distribution of spot size, the average weighting function will weight the less probable large spots the least and spots smaller than the average the most. This problem needs to be addressed. Specifically, the distribution of the beam spread is required to calculate numerically the average weighting function. It may be that this average weighting function does not significantly differ from that derived by using the RMS spread calculated from the above expressions. Another possible scenario derives from the apparently circular argument that the measurement of C_n^2 via the crossed path method requires the knowledge of the beam spread which in turn requires the knowledge of the integrated C_n^2 . The crossed path measurement may need to be made in conjunction with transverse coherence length measurements of a stellar source. These auxiliary measurements would then be used to calculate the spot size, and hence the weighting function, to enable the crossed path technique to extract altitude-resolved C_n^2 . This is an important aspect to the problem that needs to be examined further.

The other important effect of the lidar uplink propagation arises from the beam wander. The effect of beam wander is that the backscatter source separation, S_0 , becomes a random variable. The crossing altitude becomes a random variable, as does the weighting function. Wander results primarily from eddies of the same order as the beam size. If the two uplink beam are separated by a distance large with respect to the beam diameters, the wander in the two beams can be considered as statistically uncorrelated, since different eddies will be responsible for the wander in each uplink beam. The wander may be correlated at some time lag due to frozen turbulence effects, but the correlation at the same time is treated as absent. The mean square wander, $\langle \rho_c^2 \rangle$, of either a collimated or focused beam can be calculated from

$$\langle \rho_c^2 \rangle = 2.97 L^2 / (k^2 \rho_0^{5/3} D^{1/3}). \quad (114)$$

It follows that the beam wander has no wavelength dependence, since $\rho_0^{5/3}$ behaves as k^{-2} . This expression shows that wander can be reduced by increasing the transmitter diameter. Strictly, this form applies to the regime where $D > \rho_0$. For the case where $D < \rho_0$, there is negligible wander and the primary effect of turbulence is beam broadening. Wander can also be reduced by using a small enough aperture, that is, small relative to the turbulence scales. Fante²⁹ shows results from numerical calculations for the entire range of D and ρ_0 that exhibit this behavior.

As a numerical example, consider a 0.5 μm beam of 5 cm diameter at the transmitter, with receiver separation of 1 m and the nominal backscatter spot separation of 1 m. For propagation to 10 km, the nominal crossing altitude is 5 km. If the turbulence is specified in terms of 2.5 cm for

ρ_0 , the RMS wander of a single beam is calculated to be 5 cm in radius. The two uplink lidar beams are assumed to wander independently with RMS values of 5 cm, and the separation between the two spots fluctuates about the average of 1 m with an RMS value of 7 cm. This fluctuation in separation yields a fluctuation in the crossing altitude about the 5 km average by ± 175 m. Clearly, this fluctuating crossing altitude will result in an average weighting function of reduced peak magnitude and greater width than a non-fluctuating separation. The average weighting function due to wander can be calculated from the statistical distribution of wander. This will not be done here and represents an important problem for follow-up investigation. As with beam broadening, the average weighting function due to wander is needed to determine C_n^2 and generally requires knowledge of the wander, which in turn requires ρ_0 or equivalently, C_n^2 along the path. Such data can be provided by simultaneous measurements of ρ_0 .

Beam broadening and wander of the uplink lidar beam are important parameters that are required to determine the path weighting function and C_n^2 in the crossed path lidar. The impact of these parameters must be taken into account in the implementation of a system and various tradeoffs made. For example, for a narrow collimated beam of the order of a few centimeters diameter at the transmitter, wander will be less than the broadening. In effect, the beam can be considered to wander within a radius given by the broadening term. Furthermore, the diffraction broadening dominates the turbulence broadening in such cases. For such narrow transmitters, the weighting functions can be calculated using our earlier expressions using the diffraction-limited spot size; the uplink turbulence effects of wander and broadening can be ignored. This is a strong argument in favor of narrow beams. However, these diffraction-broadened beams will exceed the spot size requirements discussed earlier. Such narrow beams would result in a signal and resolution degradation. This situation is an example of the tradeoffs required in a practical system.

5. CONCLUSION

This report has demonstrated that the crossed path technique possesses unique features that can be exploited for the lidar remote sensing of C_n^2 with high spatial and temporal resolution. The uniqueness of this approach stems from the sharpness of the path weighting function. The approach is conceptually a geometric one and can be regarded as a form of intensity interferometry. Since the approach measures the normalized intensity covariance, it is less sensitive to fluctuations in laser output and laser instabilities.

There are numerous parameters, both systemic and atmospheric, to take into account in a system design. There are many tradeoffs to be made. One important class of parameters pertains to the strength of the backscattering, and hence the signal strength. This class involves the choice of wavelength and can be assessed in terms of a simulation using such existing lidar simulation codes as BACKSCAT³². The strength of the backscatter signal falls off as density in the case where Rayleigh scattering dominates. This in turn determines the integration time and the temporal resolution of the method. In order to compensate for this decrease in signal strength, the signal needs to be strengthened, perhaps by decreasing the receiver or source separations. This would degrade resolution. Ideally, the resolution of the weighting function would exactly match the

³²Guivens, N.R., Rafuse, S.E., Hummel, J.R., and Cheifetz, M.G. (1988) *BACKSCAT Lidar Backscatter Simulation User's Manual for Version 1.0*, Geophysics Laboratory, Technical Report AFGL-TR-88-0331, ADA219487.

receiver gating. With respect to the lidar formalism presented in Section 3, this situation corresponds to a diagonal weighting function matrix. If design tradeoffs require the use of broader weighting functions so that the matrix is no longer diagonal, the crossed path approach is in no way invalidated. The path weighting function is still very sharp and localized and results in a sparse matrix (that is, one which has only a few nonzero elements adjacent to the diagonal) which is readily inverted.

The outlining of the various restrictions on the system parameters seems to present many conflicts. It is doubtful that a single pair of receivers could perform an altitude profile. Rather, a single pair of receivers could be used to probe a limited altitude range, say 3 or 4 km to 7 or 8 km with a vertical resolution of 150 meters. Other pairs would be required to probe other altitude ranges; this is not regarded as a serious drawback, since the receivers consist of a telescope of a few centimeters diameter and a photomultiplier tube and are consequently relatively simple and inexpensive. The achievement of this goal of performing some prototype experiments to measure C_n^2 via the crossed path method over a limited altitude range is the test of the technique. This would demonstrate the capability to remotely sense C_n^2 with high spatial and temporal resolution, capabilities that currently do not exist.

REFERENCES

- ¹Hocking, W.K. (1986) Observation and measurement of turbulence in the middle atmosphere with a VHF radar, *J. Atmos. and Terres. Physics*, 48:655-670.
- ²Green, J.L., Beland, R.R., Brown, J.H., Clark, W.L., Eaton, F.D., Favier, L.D., Gage, K.S., Hatch, W.H., Hines, J.R., Murphy, E.A., Nastrom, G.D., Peterson, W.A., VanZandt, T.E., and Warnock, J.M. (1989) Comparisons of Refractivity Measurements from the Flatlands VHF Radar with Other Measurement Techniques, Proceedings of the 24th Conference on Radar Meteorology, Tallahassee, FL.
- ³Eaton, F.D., Peterson, W.A., Hines, J.R., Peterman, K.R., Good, R.E., Beland, R.R., and Brown, J.H. (1988) Comparisons of VHF radar, optical and temperature fluctuation measurements of C_n^2 , ϵ_0 , and θ_0 , *Theor. Appl. Climatol.*, 39:17-29.
- ⁴Brown, J.H., Good, R.E., Bench, P.M., and Faucher, G. (1982) *Sonde Measurements for Comparative Measurements of Optical Turbulence*, Air Force Geophysics Lab., AFGL-TR-82-0079, ADA118740.
- ⁵Walters, D.L., Weitekamp, M.R., Beland, R.R., Good, R.E., and Murphy, E.A. (1990) Single Probe Optical Turbulence Profile Measurement System, Symposium on Propagation Through Turbulence, Annual Meeting of the Opt. Soc. Am., Boston, MA.
- ⁶Krause-Polstorff, J., and Walters, D.L. (1990) Refractive turbulence profiling using an orbiting light source, *Appl. Opt.*, 29:1877-1885.
- ⁷Azouit, M., Vernin, J., Barletti, R., Ceppatelli, G., Righini, A., and Speroni, N. (1980) Remote sensing of atmospheric turbulence by means of a fast optical method: A comparison with simultaneous *in situ* measurements, *J. Appl. Meteor.*, 19:834-838.
- ⁸Dahlquist, G., and Bjorck, A. (1974) *Numerical Methods*, Prentice-Hall, Englewood Cliffs, N.J.
- ⁹Sasiela, R.J. (1988) *A Unified Approach to Electromagnetic Wave Propagation in Turbulence and the Evaluation of Multiparameter Integrals*, Technical Report No. 807, MIT/Lincoln Laboratory.
- ¹⁰Ochs, G.R., and Wang, T. (1978) Finite aperture scintillometer for profiling wind and C_n^2 , *Appl. Opt.*, 17:3774-3778.
- ¹¹Vernin, J., and Pelon, J. (1986) Scidar/lidar description of a gravity wave and associated turbulence: preliminary results, *Appl. Opt.*, 25:2874-2877.
- ¹²Wang, T., Clifford, S.F., and Ochs, G.R. (1974) Wind and Refractive-Turbulence Sensing Using Crossed Laser Beams, *Appl. Opt.*, 13:2602-2608.

- ¹³Fisher, M.J., and Krause, F.J.(1967) The crossed-beam correlation technique, *J. Fluid Mech.*, 28:705-717.
- ¹⁴Fried, D.L. (1967) Aperture Averaging of Scintillations, *J. Opt. Soc. Am.*, 57:169-175.
- ¹⁵Clifford, S.F. (1978) The Classical Theory of Wave Propagation in a Turbulent Medium, Chapter 2, in *Laser Beam Propagation in the Atmosphere*, J.W. Strohbehn, Ed., Springer-Verlag, New York.
- ¹⁶Tatarski, V.I. (1961) *Wave Propagation in a Turbulent Medium*, McGraw-Hill, New York.
- ¹⁷Mathews, J., and Walker, R.L. (1970) *Methods of Mathematical Physics*, 2nd edn., W.A. Benjamin, Reading, MA.
- ¹⁸Bracewell, R.N. (1978) *The Fourier Transform and Its Applications*, 2nd edn., McGraw-Hill, N.Y.
- ¹⁹Ishimaru, A. (1978) *Wave Propagation and Scattering in Random Media*, Vol. 2, Academic Press, N.Y.
- ²⁰Hill, R.J., and Clifford, S.F. (1978) Modified spectrum of atmospheric temperature fluctuations and its application to optical propagation, *J. Opt. Soc. Am.*, 68:892-899.
- ²¹Hill, R.J. (1983) Inner-scale effect on the irradiance of light propagating in atmospheric turbulence, in *Laser Beam Propagation in the Atmosphere*, *Proc. of the SPIE*, 410.
- ²²Hocking, W.K. (1985) Measurement of turbulent energy dissipation rates in the middle atmosphere by radar techniques: A review, *Radio Sci.*, 20:1403-1422.
- ²³Barat, J. (1982) Some Characteristics of Clear-Air Turbulence in the Middle Stratosphere, *J. Atmos. Sci.*, 39:2553-2564.
- ²⁴Lee, R.E., and Harp, J.C. (1969) Weak Scattering in Random Media, with Applications to Remote Probing, *Proc. IEEE*, 57:375-406.
- ²⁵Roddier, C., and Vemin, J. (1977) Relative contribution of upper and lower atmosphere to integrated refractive-index profiles, *Appl. Opt.*, 16:2252-2256.
- ²⁶Rocca, A., Roddier, F., and Vemin, J. (1974) Detection of atmospheric turbulence layers by spatiotemporal and spatioangular correlation measurements of stellar-light scintillation, *J. Opt. Soc. Am.*, 64:1000-1004.
- ²⁷Azouit, M., and Vemin, J. (1980) Remote Investigation of Tropospheric Turbulence by Two-Dimensional Analysis of Stellar Scintillation, *J. Atmos. Sci.*, 37:1550-1557.

²⁸Hill, R.J. (1988) Comparison of scintillation methods for measuring the inner scale of turbulence, *Appl. Opt.*, 47:2187-2193.

²⁹Fante, R.L. (1975) Electromagnetic Beam Propagation in a Turbulent Media, *Proc. IEEE*, 63: 1669-1692.

³⁰Yura, H.T. (1971) Atmospheric Turbulence Induced Laser Beam Spread, *Appl. Opt.*, 10:2771-2773.

³¹Fried, D.L. (1966) Optical Resolution Through a Randomly Inhomogeneous Medium, *J. Opt. Soc. Am.*, 56:1372-1379.

³²Guivens, N.R., Rafuse, S.E., Hummel, J.R., and Cheifetz, M.G. (1988) *BACKSCAT Lidar Backscatter Simulation User's Manual for Version 1.0*, Geophysics Laboratory, Technical Report AFGL-TR-88-0331, ADA219487.